

# ***SiC/SiC Cladding Materials Properties Handbook***

**Nuclear Technology  
Research and Development**

***Prepared for  
U.S. Department of Energy  
Nuclear Technology Research and  
Development Advanced Fuels Campaign  
T. Koyanagi<sup>1</sup>, Y. Katoh<sup>1</sup>, G. Singh<sup>1</sup>  
M. Snead<sup>2</sup>***

***<sup>1</sup>Oak Ridge National Laboratory  
<sup>2</sup>Brookhaven National Laboratory***

***August 2017***

**M3-FT17OR020202104**





**DISCLAIMER**

This information was prepared as an account of work sponsored by an agency of the U.S. Government. Neither the U.S. Government nor any agency thereof, nor any of their employees, makes any warranty, expressed or implied, or assumes any legal liability or responsibility for the accuracy, completeness, or usefulness, of any information, apparatus, product, or process disclosed, or represents that its use would not infringe privately owned rights. References herein to any specific commercial product, process, or service by trade name, trade mark, manufacturer, or otherwise, does not necessarily constitute or imply its endorsement, recommendation, or favoring by the U.S. Government or any agency thereof. The views and opinions of authors expressed herein do not necessarily state or reflect those of the U.S. Government or any agency thereof.



## SUMMARY

When a new class of material is considered for a nuclear core structure, the in-pile performance is usually assessed based on multi-physics modeling in coordination with experiments. This report aims to provide data for the mechanical and physical properties and environmental resistance of silicon carbide (SiC) fiber-reinforced SiC matrix (SiC/SiC) composites for use in modeling for their application as accident-tolerant fuel cladding for light water reactors (LWRs). The properties are specific for tube geometry, although many properties can be predicted from planar specimen data. This report presents various properties, including mechanical properties, thermal properties, chemical stability under normal and off-normal operation conditions, hermeticity, and irradiation resistance. Table S.1 summarizes those properties mainly for nuclear-grade SiC/SiC composites fabricated via chemical vapor infiltration (CVI). While most of the important properties are available, this work found that data for the in-pile hydrothermal corrosion resistance of SiC materials and for thermal properties of tube materials are lacking for evaluation of SiC-based cladding for LWR applications.

Table S.1. Summary of CVI SiC/SiC properties with a tube geometry

| Properties                        | Nonirradiated  | Neutron-irradiated   |
|-----------------------------------|--|--|
| Density                           | 2.6–2.8 g/cm <sup>3</sup>  | Up to ~2% volumetric swelling at ~300°C (Figure 14)                            |
| Porosity                          | 8–17%  | No change expected   |
| Fiber volume fraction             | 30–40 %  | No change expected   |
| Coefficient of thermal expansion  | Eq. (1)  | No change by irradiation   |
| Thermal diffusivity               | Material dependent (Table 5)   | Estimated from data obtained from plate specimen (Figure 16)                   |
| Specific heat                     | Same as chemical vapor deposited (CVD) SiC   | No change expected   |
| Gas leak tightness                | Table 6  | He and D <sub>2</sub> leak tight following neutron irradiation (CVD SiC layer) |
| Young's modulus                   | ~160 GPa (hoop); see Figure 4 (axial)  | Insignificant irradiation effect   |
| Poisson's ratio                   | 0.13 at 0/90° to 0.25 at ±45° fiber orientation from loading direction (in-plane, plate specimen)  | Insignificant irradiation effect expected                                      |
| Proportional limit stress         | 80–100 MPa (axial); 100–160 MPa (hoop)   | Insignificant irradiation effect   |
| Ultimate strength                 | See Figure 5 and Figure 6  | Insignificant irradiation effect   |
| Statistical strength              | Weibull modulus $m \sim 10$ (axial UTS), axial PLS follows log-normal distribution with log-mean and log-standard deviation as 4.52 and 0.096 respectively | No data available  |
| Hydrothermal corrosion resistance | Water chemistry-dependent weight loss (Figure 7)   | Limited data available   |
| Compatibility with fuel           | Insignificant reaction under a normal operation condition  | Expected insignificant reaction under a normal operation condition             |
| Steam oxidation resistance        | At least one order of magnitude smaller thickness consumption of SiC than Zr (Figure 10)   | No data available  |

This page is intentionally left blank.

## CONTENTS

|   |     |
|---|-----|
| SUMMARY .....   | iii |
| FIGURES .....   | vii |
| TABLES .....  | iii |
| ABBREVIATIONS, ACRONYMS, AND INITIALISMS .....                                  | iv  |
| 1. INTRODUCTION .....   | 1   |
| 1.1 Background .....  | 1   |
| 1.2 Document Purpose .....  | 1   |
| 1.3 Product Forms Covered .....   | 2   |
| 1.4 Specifications and Standards.....   | 3   |
| 2. DESIGN AND MANUFACTURE .....   | 3   |
| 2.1 Fibers.....   | 3   |
| 2.1.1 Fiber type .....  | 3   |
| 2.1.2 Fiber architecture .....  | 3   |
| 2.2 Interphase.....   | 4   |
| 2.3 Matrix.....   | 5   |
| 2.3.1 CVI matrix .....  | 5   |
| 2.3.2 NITE matrix .....   | 6   |
| 2.4 Coatings .....  | 6   |
| 2.5 Joints .....  | 7   |
| 2.5.1 Solid state diffusion bonding .....                                       | 7   |
| 2.5.2 Metallic braze-based joining .....  | 8   |
| 2.5.3 Glass ceramics joining .....  | 8   |
| 2.5.4 Joining using SiC pre-ceramics precursors .....                           | 8   |
| 2.5.5 Reaction sintering with Si-C and Ti-Si-C systems .....                    | 8   |
| 2.5.6 Liquid-phase sintering of SiC .....                                       | 8   |
| 2.5.7 Selected-area chemical vapor deposition/infiltration.....                 | 9   |
| 2.5.8 Other methods.....  | 9   |
| 3. NONIRRADIATED MATERIAL PROPERTIES .....                                      | 9   |
| 3.1 Physical and Thermal Properties.....  | 9   |
| 3.1.1 Density, porosity, and fiber volume fraction .....                        | 9   |
| 3.1.2 Thermal expansion.....  | 12  |
| 3.1.3 Thermal diffusivity .....   | 12  |
| 3.1.4 Specific heat.....  | 13  |
| 3.1.5 Gas leak tightness.....   | 13  |
| 3.2 Mechanical Properties.....  | 15  |
| 3.2.1 Young’s modulus .....   | 15  |
| 3.2.2 Proportional limit stress .....   | 19  |
| 3.2.3 Ultimate tensile strength .....   | 19  |
| 3.2.4 Strain at proportional limit strength and ultimate tensile strength ..... | 21  |
| 3.2.5 Poisson’s Ratio.....  | 21  |

---

|       |   |    |
|-------|---|----|
| 3.3   | Corrosion, Oxidation and Fuel Compatibility.....  | 21 |
| 3.3.1 | Hydrothermal corrosion.....                       | 21 |
| 3.3.2 | Fuel-clad chemical interaction.....               | 25 |
| 3.3.3 | Steam oxidation.....                              | 25 |
| 4.    | IRRADIATED MATERIAL PROPERTIES.....               | 26 |
| 4.1   | Physical and Thermal Properties.....              | 26 |
| 4.1.1 | Density.....                                      | 26 |
| 4.1.2 | Fiber volume fraction and porosity.....           | 31 |
| 4.1.3 | Thermal expansion.....                            | 31 |
| 4.1.4 | Thermal diffusivity and thermal conductivity..... | 32 |
| 4.1.5 | Specific heat.....                                | 33 |
| 4.1.6 | Permeability.....                                 | 33 |
| 4.2   | Mechanical Properties.....                        | 34 |
| 4.3   | In-Pile Hydrothermal Corrosion.....               | 37 |
| 5.    | FUTURE DIRECTION.....                             | 38 |
| 6.    | ACKNOWLEDGMENTS.....                              | 38 |
| 7.    | REFERENCES.....                                   | 38 |



## FIGURES

|   |    |
|---|----|
| Figure 1. Examples of the fiber architecture of a CVI SiC/SiC tube: (a) filament winding, (b) 2D braiding, and (c) 3D braiding. Reprinted from Sauder 2014 [12].  | 4  |
| Figure 2. Examples of monolayer PyC interphase (left) and multilayer PyC interphase (right).  | 5  |
| Figure 3. Specific heat of SiC at elevated temperatures [61].   | 13 |
| Figure 4. Axial Young's moduli determined from several studies for CVI SiC/SiC tubes.   | 16 |
| Figure 5. Axial UTS determined from several studies for CVI SiC/SiC tubes.  | 20 |
| Figure 6. Hoop UTS determined from several studies for CVI SiC/SiC tubes.   | 20 |
| Figure 7. Mass change in CVD SiC after exposure to simulated reactor water loops [66, 67].  | 22 |
| Figure 8. Linear mass loss rate for NITE SiC with various sintering additives, CVD-SiC, and polycrystalline alumina [26]. The corrosion test was conducted for up to 3 months for CVD SiC, 2 months for YA-NITE, and 5 weeks for the other materials. YA-NITE, CZA-2-NITE, and YZA-NITE are NITE ceramics fabricated with sintering additives of $Y_2O_3-Al_2O_3$ , $CeO_2-ZrO_2-Al_2O_3$ , and $Y_2O_3-ZrO_2-Al_2O_3$ systems, respectively. | 23 |
| Figure 9. Cross-sectional observation of SiC joints after autoclave immersion: (a) molybdenum diffusion bond tested with BWR-HWC for 5 weeks and (b) nanopowder sintered SiC joint tested with BWR-NWC for 5 weeks [45].  | 24 |
| Figure 10. Thickness consumed (in $\mu m$ ) during steam oxidation: (a) Zircaloy-4 and (b, c) CVD SiC. (Reprinted from Terrani 2014 [3]).   | 25 |
| Figure 11. Representative image of test specimens used for irradiation experiment. Length of all specimens was 25 mm. Details for each material are shown in Table 9.   | 26 |
| Figure 12. Linear swelling of CVD SiC and SiC/SiC plates. Details for the materials investigated are shown in Table 9.  | 27 |
| Figure 13. Anisotropic swelling of CVI SiC/SiC plates. The relationship between specimen direction and fiber architecture is shown in Table 9.  | 29 |
| Figure 14. Temperature and dose dependence of swelling of CVD SiC and CVI SiC/SiC composites.   | 30 |
| Figure 15. Instantaneous CTE of neutron-irradiated CVI SiC/SiC composite plates. The black line is the trend of nonirradiated materials, which is described in Eq. (1). The material information can be found in Table 9.   | 31 |
| Figure 16. Room-temperature radiation defect thermal resistivity of neutron-irradiated SiC/SiC composites and monolithic CVD SiC plotted against irradiation temperature [6, 8]. The neutron dose ranged from 0.8 to 11.7 dpa for composites.   | 32 |
| Figure 17. (a) Helium and (b) deuterium permeation fluxes through neutron-irradiated CVD SiC as a function of applied gas pressure. [64]  | 34 |
| Figure 18. Flexural stress strain curves for (a) CVI SiC/SiC (HNS)-C and (b) CVI SiC/SiC (SA3) for nonirradiated and irradiated conditions [85]. The specimen information can be found in Table 9.  | 36 |

This page is intentionally left blank.

## TABLES

|  |     |
|--|-----|
| Table S.1. Summary of CVI SiC/SiC properties with a tube geometry.....   | iii |
| Table 1. Examples of SiC/SiC composite configurations.....   | 2   |
| Table 2. SiC/SiC tube configurations considered for material handbook.....   | 2   |
| Table 3. Joining technologies available for SiC.....   | 7   |
| Table 4. Summary of different SiC/SiC tubes and their physical properties.....   | 10  |
| Table 5. Through-thickness thermal diffusivity of CVI SiC/SiC tubes evaluated using a laser flash method.....  | 12  |
| Table 7. Compilation of mechanical properties of SiC/SiC composite determined from tests on tube specimens.....  | 17  |
| Table 8. Hydrothermal corrosion resistance of coated materials. The coated zirconium-based alloy was tested unless otherwise indicated.....  | 24  |
| Table 9. Information for CVD SiC and SiC/SiC composite materials used for swelling measurements.....   | 27  |
| Table 10. Mechanical properties of CVI SiC/SiC composites nonirradiated and irradiated under LWR-relevant temperature and dose conditions. All the irradiation experiments were carried out under an inert gas atmosphere in the HFIR..... | 35  |
| Table 11. Apparent shear strength of various SiC joints with and without irradiation. The substrate was monolithic CVD SiC for all cases. Torsion tests using a miniature hourglass specimen were conducted to obtain the data.....        | 37  |

## ABBREVIATIONS, ACRONYMS, AND INITIALISMS

| Acronym | Description                                | Acronym | Description                                    |
|---------|--|---------|--|
| °C      | Degree Celsius                             | LVDT    | Linear variable differential transformer       |
| 2D      | Two dimensional                            | LWR     | Light water reactor                            |
| 3D      | Three dimensional                          | Li      | Lithium  |
| Ag      | Silver                                     | Mg      | Magnesium                                      |
| Al      | Aluminum                                   | MPa     | Megapascal                                     |
| ASTM    | American Society for Testing and Materials | NITE    | Nano-infiltration and transient eutectic phase |
| ATC     | Accident-tolerant cores                    | O       | Oxygen   |
| ATF     | Accident tolerant fuels                    | OD      | Outer diameter                                 |
| B       | Boron                                      | PLS     | Proportional limit stress                      |
| C.V.    | Coefficient of variance                    | PVD     | Physical vapor deposition                      |
| cm      | Centimeter                                 | PyC     | Pyrolytic carbon                               |
| CMC     | Ceramic matrix composite                   | Ref.    | Reference                                      |
| Cu      | Copper                                     | SA3     | Tyranno SA3                                    |
| CVD     | Chemical vapor deposition                  | Si      | Silicon  |
| CVI     | Chemical vapor infiltration                | SiC     | Silicon carbide                                |
| EBC     | Environmental barrier coating              | Ti      | Titanium                                       |
| FCCI    | Fuel-clad chemical interaction             | UTS     | Ultimate tensile strength                      |
| g       | gram                                       | VPS     | Vacuum plasma spray                            |
| GPa     | Gigapascal                                 | Y       | Yttrium  |
| HNS     | Hi-Nicalon Type S                          | Zr      | Zirconium                                      |
| HS      | hermetic sealing                           |         |  |
| IBN     | Sylramic™ fiber                            |         |  |
| ID      | Inner diameter                             |         |  |

# SIC/SIC CLADDING MATERIALS PROPERTIES HANDBOOK

## 1. INTRODUCTION

### 1.1 Background

Fuels and core structures in current light water reactors (LWRs) are vulnerable to catastrophic consequences in the event of loss of coolant or active cooling, as was evidenced by the March 2011 Fukushima Dai-ichi Nuclear Power Plant accident [1, 2]. This vulnerability is attributed primarily to the rapid oxidation kinetics of zirconium (Zr) alloys in a water vapor environment at very high temperatures, which results in the production of explosive hydrogen [3]. Current LWRs use Zr alloys nearly exclusively as materials for fuel cladding and core structures. Silicon carbide (SiC) –based materials, in particular continuous SiC fiber–reinforced SiC matrix ceramic composites (SiC/SiC composites or SiC composites) are among the candidate alternative materials for LWR fuel cladding and core structures to enable so-called accident-tolerant fuels (ATFs) and accident-tolerant cores. SiC and SiC/SiC composites are considered to provide outstanding passive safety features in beyond-design-basis severe accident scenarios [2, 3]. SiC/SiC composites are anticipated to provide additional benefits over Zr alloys: smaller neutron absorption cross sections, general chemical inertness, ability to withstand higher fuel burn-ups and higher temperatures, exceptional inherent radiation resistance, lack of progressive irradiation growth, and low induced activation/low decay heat [4]. Moreover, SiC is considered to be permanently stable in nuclear waste [4]. Although SiC-based cladding appears to be attractive, critical feasibility issues such as (1) hydrothermal corrosion, (2) potential loss of fission gas retention due to cracking under normal operation conditions, and (3) development of fuel performance modeling capability, must be addressed [5]. This report is related to the issue of modeling capability. For successful development of SiC-based cladding, such fuel performance modeling plays critical roles, as explained in Section 1.2.

### 1.2 Document Purpose

After decades of experience with metallic cladding components in thermal and fast reactors, the transition to using SiC ceramic matrix composites represents a revolutionary paradigm shift. Because of the impact associated with any such transition, associated challenges will need to be carefully assessed via predictive fuel performance analysis. Fuel performance analysis tools guide the design process to optimize performance for the integral fuel module under normal and off-normal operating conditions. Note that the term “fuel,” as used herein, refers to the integral structure consisting of the pellet, the cladding, and other fuel assembly components.

Although the properties of SiC/SiC composites, including the effects of neutron irradiation, are relatively well understood as a candidate fuel cladding material [6], they have been insufficiently incorporated in fuel performance models and core designs. There are several reasons for this, including the intrinsic behavioral differences between ceramic composites and metallic alloys, the tailorable and anisotropic nature of composite properties, and the complexity of interactions among irradiation-induced evolutions of thermophysical properties. To achieve improved fidelity for comprehensive performance modeling and analysis of fuel systems involving SiC/SiC cladding, properties of these composites in small-diameter tubular geometries are compiled and analyzed in this report. The properties data analysis and interpretation are discussed in relation to the constitutive modeling, effects of neutron irradiation, predictive capability, and critical deficiencies in data and knowledge.

The intent of this document is to summarize the material properties available for as-manufactured and irradiated SiC/SiC composite fuel cladding in the form of thin tubes. If data are not yet available, SiC/SiC plate data are given with an explanation on how it would apply to tubes.

### 1.3 Product Forms Covered

The SiC/SiC composites analyzed in this report are limited to continuous and near-stoichiometric SiC fiber-reinforced composites with fully crystalline SiC matrices. The SiC/SiC composite-based fuel claddings that are currently considered for LWRs include fully ceramic composite cladding, layered cladding consisting of any combination of SiC composite and monolithic SiC layers, and a variety of ceramic-metal hybrid concepts that use SiC/SiC composites as the primary structural element and a compliant metal to aid in fission product retention (see Table 1 for examples). Other functions of these layers include hermetic sealing (HS) and environmental barrier coatings (EBCs).

Table 1. Examples of SiC/SiC composite configurations

| Class                   | Layer configuration (from inner to outer) | Configuration | Remarks  | Reference     |
|-------------------------|---|---------------|--|---------------|
| Full ceramics           | Composite                                 |               | Monolithic surface layer may present   | [7]           |
|                         | Composite-monolith                        | Duplex        | Monolithic layer as HS/EBC against hydrothermal corrosion                    | [8]           |
|                         | Monolith-composite                        | Duplex        | Monolithic layer as HS/EBC against fuel-cladding chemical interaction (FCCI) | [7]           |
|                         | Monolith-composite-monolith               | Triplex       | Monolithic layer as HS/EBC against hydrothermal corrosion and FCCI           | [9]           |
| Metal-assisted ceramics | Metal-composite                           | Duplex        | Metallic layer as HS/EBC against FCCI  | [10]          |
|                         | Composite-metal                           | Duplex        | Metallic layer as HS/EBC against hydrothermal corrosion                      | [11]          |
|                         | Metal-composite-metal                     | Triplex       | Metallic layer as HS/EBC against hydrothermal corrosion and FCCI             | Not available |
|                         | Composite-metal-composite                 | Triplex       | Metallic layer as HS   | [12]          |

Multiple types of SiC/SiC cladding tubes are available, manufactured with different combinations of fibers, interphases, matrices, and architectures. Table 2 lists the SiC/SiC clad tubes under consideration for this material handbook.

Table 2. SiC/SiC tube configurations considered for material handbook

| Type   | Fiber   | Interphase       | Matrix  |
|--------|---|------------------|---|
| Type 1 | HNS fiber   | Pyrolytic carbon | Chemical vapor infiltrated (CVI) SiC          |
| Type 2 | SA3 fiber   | Pyrolytic carbon | CVI SiC                                       |
| Type 3 | SA3 fiber   | Pyrolytic carbon | Nano-infiltration and transient eutectoid SiC |
| Type 4 | All tubes that do not fall under Types 1–3, e.g., IBN fiber |                  |   |

## 1.4 Specifications and Standards

There is no standard manufacturing specification for SiC/SiC tubes because standards are still under development. ASTM C1783-15, “Standard Guide for Development of Specifications for Fiber Reinforced Silicon Carbide-Silicon Carbide Composite Structures for Nuclear Applications,” is a guide for preparing material specifications for SiC/SiC composite structures (flat plates, rectangular bars, round-rods, and tubes) that are manufactured specifically for structural components and for fuel cladding in nuclear reactor core applications. This standard also recommends ASTM standards according to which the physical, mechanical, and durability properties should be measured.

## 2. DESIGN AND MANUFACTURE

The following are the general manufacturing steps for SiC/SiC cladding:

1. SiC fibers are braided/knitted/stitched into 3-dimensional (3D) tubes, referred to as the architecture of the tubes.
2. An interphase layer is added by chemical vapor deposition (CVD).
3. The matrix is added by either chemical vapor infiltration (CVI) or by nano-infiltration transient eutectic phase (NITE) sintering using hot pressing.
4. Inner or outer coating layers may be added using different techniques.

The composite properties are to a large extent determined by the volume fractions and orientations of the fibers in relation to the orientation of interest for certain properties [6].

The following sections describe the design and manufacture of SiC/SiC composite fuel cladding. Their purpose is to give the reader some background to aid understanding of how each manufacturing component can influence the material properties of the final tube.

### 2.1 Fibers

#### 2.1.1 Fiber type

Nuclear-grade SiC fiber is considered near-stoichiometric and highly crystalline because of its dimensional stability under irradiation compared with non-stoichiometric and amorphous-like SiC fibers [6, 13]. This generation III class of SiC fibers includes Hi-Nicalon Type S (HNS; Nippon Carbon Co., Tokyo, Japan) [14, 15], Tyranno SA3 (SA3; Ube Industries Ltd., Ube, Japan) [16], and Sylramic (IBN; COI Ceramics, San Diego) [17]. The properties of these fibers can be found elsewhere [6, 18]. Briefly, they have similar mechanical properties: Young’s modulus of ~400 GPa and room temperature tensile strength of >2 GPa, but their thermal properties may differ significantly. The effect of the fiber on the properties of the tube is highly dependent on the fiber architecture.

#### 2.1.2 Fiber architecture

Given certain properties for the constituent materials, the composite properties are determined by the fiber architecture. The reinforcing fibers provide benefits such as strength and toughness most effectively in directions parallel to the fiber axis. More precisely, the composite properties are to a large extent determined by the volume fractions and orientations of the fibers in relation to the orientation of interest

for certain properties. Therefore, tailoring the fiber architecture is a key to optimizing the cladding mechanical properties [6]. Examples of fiber architecture are shown in Figure 1.

The common fiber architectures include two direction (2D) layups in the form of woven fabrics, 2.5D layups with cross weaving through the woven fabrics, 3D orthogonal weaves. In addition, braiding (both 2D and 3D) preforms have become popular [12] because of the high level of conformability and damage resistance. 2D braided preforms are composed of intertwined fiber structures capable of  $0^\circ$  and  $\pm\theta$  layups. 3D braiding preforms are produced by intertwining or orthogonal interlacing of yarns to form an integral structure through position placement thereby providing through-thickness reinforcement as well as being readily adaptable to a wide range of complex shapes.

The different fiber architecture was reported to result in different fiber volume fraction and size and distribution of pores [12], which greatly affects the thermomechanical properties of the composites. The effects of fiber architecture on the mechanical properties are shown and discussed in section 3.2.

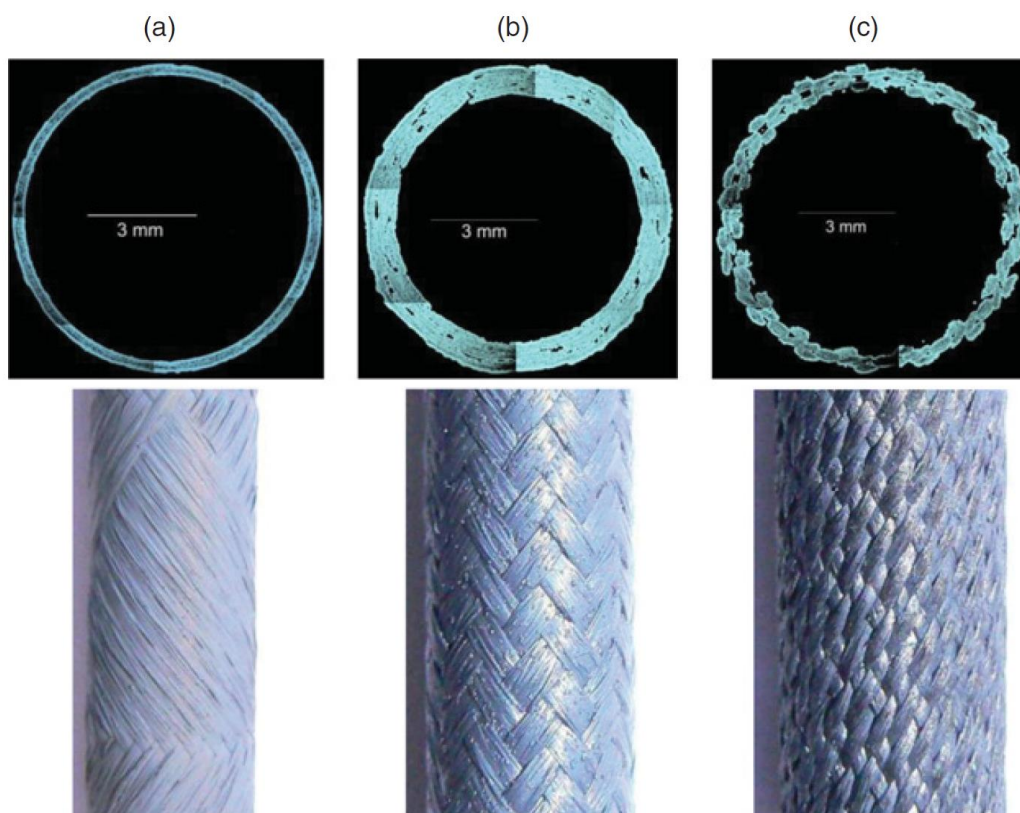


Figure 1. Examples of the fiber architecture of a CVI SiC/SiC tube: (a) filament winding, (b) 2D braiding, and (c) 3D braiding. Reprinted from Sauder 2014 [12].

## 2.2 Interphase

SiC/SiC composites are engineered materials particularly attractive for their tailorable, predictable, and reliable mechanical properties and excellent damage tolerance. The advantages of SiC/SiC composites are enabled by their fiber-matrix interface with adequate bonding strength and interfacial sliding strength. The primary tough fracture behavior of the ceramic composite is realized through the deflection of matrix



cracks at the fiber/matrix interface without the breaking of fibers followed by fiber pull-out that is associated with frictional dissipation. Carbon-based interphases, such as the monolayer pyrolytic carbon (PyC) interphase and the multi-layer PyC/SiC interphase (Figure 2), are proven to be irradiation resistant [6]. The interphase is typically formed via a CVD process. The interphase thickness has been reported to slightly affect mechanical properties such as ultimate tensile strength (UTS), proportional limit stress (PLS), Young's modulus, and strain to failure when plate specimens were tested [19]. No systematic investigation of the effects of the interphase thickness on the mechanical properties of tubular SiC/SiC materials has been reported.

Boron nitride (BN) might be another option for the interphase material [18] if isotropically controlled  $^{11}\text{B}$  is used to eliminate the  $^{10}\text{B}$  content to avoid boron burnup and the production of transmutant helium by  $^{10}\text{B}(n, \alpha)^7\text{Li}$  reactions during irradiation.

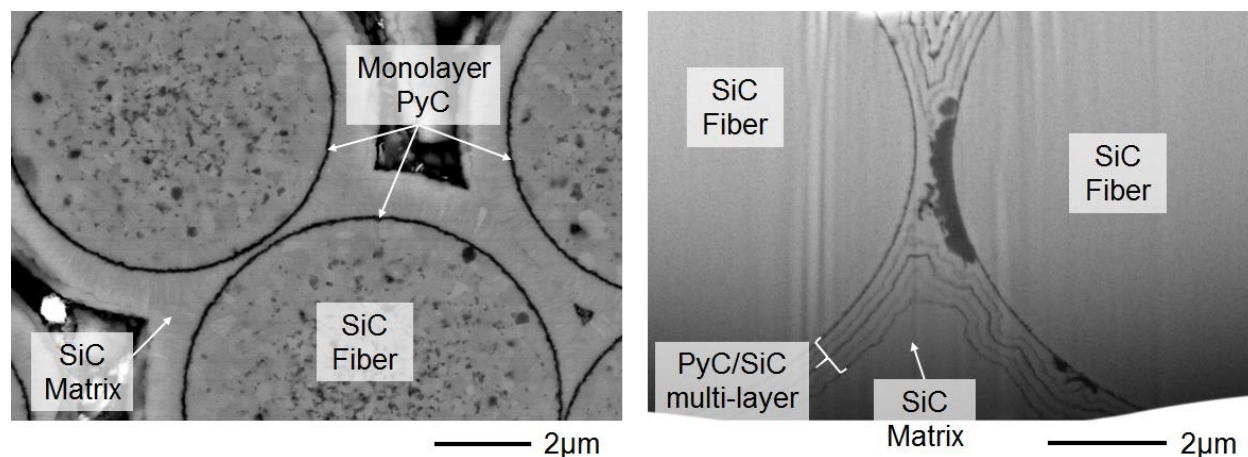


Figure 2. Examples of monolayer PyC interphase (left) and multilayer PyC interphase (right).

## 2.3 Matrix

SiC/SiC composite densification routes that have been proved to produce radiation-resistant forms of composite materials are CVI and SiC powder sintering sintering represented by the NITE (nano-infiltration and transient eutectic phase) process. CVI SiC/SiC is a mature technology that has already demonstrated scale components with reasonable reproducibility up to large dimensions [18]. Experience with NITE SiC/SiC is more limited, but the fabrication of SiC/SiC composites of complex shapes—such as variable-diameter combustor liners, heat exchangers, and screw-ended tubes—has been demonstrated [20, 21]. The manufacture of thin-walled tubes with a large length-to-diameter ratio remains a challenge for both fabrication routes.

### 2.3.1 CVI matrix

CVI is the most reliable method of producing a matrix composed of the very high-purity, crystalline SiC that is necessary to provide good irradiation resistance for nuclear applications [6]. For a CVI process, manufacturing such tubes will require a large production facility that achieves adequate uniformity in temperature distribution and reactant flow conditions along the full tube length, which is technically not very difficult but will require a substantial capital investment.

The deposition rate is one of the key processing parameters. High deposition rates during composite fabrication leads to high levels of internal porosity. Low deposition rates are required to achieve low internal porosity, but they result in long fabrication times. Increasing the internal density of the matrix leads to improved mechanical and thermal properties [22].

Recently, General Atomics became capable of producing ~1 m long tubes via CVI with adequate straightness, wall thickness uniformity, roundness, and reproducibility of surface roughness [7]. A Toshiba-Ibiden-Tohoku University team in Japan has developed a CVD/CVI facility that is capable of manufacturing prototype channel boxes and is in the process of expanding that process to manufacture full-length (~4 m) components [23].

Alternative methods for the manufacture of tubes with extreme length-to-diameter ratios, such as segmented tube fabrication, may also be considered. Options may include adhesive joining or mechanical fastening of shorter tubes to make full-length fuel rods, or modifying the fuel assembly design to accommodate axially stacked shorter fuel rods that are individually sealed.

### 2.3.2 NITE matrix

The NITE process has demonstrated an almost fully dense SiC/SiC composite [24]. This achievement is beneficial to the fabrication of a gas-leaktight cladding without any additional processing such as a CVD SiC coating. NITE is a specific type of liquid-phase sintering for SiC/SiC composites: sintering of SiC fiber forms infiltrated with an SiC slurry consisting of an SiC powder with nanosize particles and oxide additives such as a eutectic composition of alumina and yttria [24]. NITE SiC/SiC tubes may be produced by a hot isostatic press, using a furnace of adequate size. A 20 cm long tube has been fabricated for irradiation in a material testing reactor [25].

Since the NITE matrix contains secondary phases attributed to the oxide additives, a key challenge for the LWR cladding application is achieving a matrix resistant to reactor environments, including hydrothermal corrosion for normal operation and high-temperature steam oxidation for accident conditions. The secondary phases along the grain boundaries and grain pockets are preferentially attacked under a hydrothermal corrosion environment [26].

## 2.4 Coatings

At normal operating conditions, depending on the water chemistry, SiC may corrode at an unacceptable rate. As a ceramic matrix composite material, it is expected to undergo microcracking under normal stress conditions, based on statistical probability; the cracking may compromise its ability to contain gaseous fission products. A possible solution to both issues is the application of mitigating coatings on the outer surface of the cladding for use in normal operating conditions. Such an environmental barrier coating (EBC) to prevent hydrothermal corrosion is being actively developed for Zr-based cladding [27]. For SiC/SiC composites, the EBC is a familiar way of improving high-temperature corrosion resistance for turbine applications [28]. However, there has been only limited development of EBCs for LWR SiC claddings. Coating technologies reported in the literature include electrochemical deposition of chromium; cathodic arc physical vapor-deposited Cr, CrN, and TiN; and vacuum plasma-sprayed Cr and Zr [11]. Note that current EBC technology for ATF SiC/SiC cladding is immature, and future work should include demonstrations of hydrothermal corrosion resistance and hermeticity.

## 2.5 Joints

For the successful development of SiC-based fuel cladding, joining of the cladding to the end-plug is recognized as a technological hurdle [2, 29]. This issue is specific to pin-type nuclear fission fuels. The functional requirements for the joint are (1) gastightness to retain fission products inside the cladding; (2) environmental resistance, i.e., resistance to hydrothermal corrosion and neutron irradiation, under normal operating conditions; and (3) high-temperature steam oxidation resistance under loss-of-coolant accident conditions. The performance of the joint is expected to be highly dependent on the bonding layer and the end-plug geometry.

The end-plug geometry may depend on the joining process and cladding material. Butted [30, 31], scarf [31], and butted scarf [31] end-plugs have been demonstrated. A screw type end-plug was employed in a case in which a machinable NITE SiC/SiC composite was used [25]. Generally, a larger bonding area yields superior mechanical properties, gas leaktightness, and corrosion/oxidation resistance. However, an end-plug and a cladding with relatively complex geometries will be required to achieve an incrementally larger bonding area.

There are various options for joining SiC to SiC, although limited literature was found for joining end-plug and tube materials. Representative joining processes are listed in Table 3, and each is briefly described in the following subsections. Note that one of the processing difficulties regarding end-cap joining for a long cladding with thin walls is a limitation in the applied stress that can be employed during joining. In addition, the joining temperature should be low enough to avoid impacting the composite properties by annealing. The strengths of HNS and SA3 SiC fibers are known to degrade under annealing at  $\sim 1800^{\circ}\text{C}$  and  $\sim 1900^{\circ}\text{C}$ , respectively [32].

Table 3. Joining technologies available for SiC

| Joining method                                   | Bonding layer   | Processing conditions   |
|--|---|---|
| Solid state diffusion bonding                    | None or refractory metallic foils such as titanium and molybdenum | $\sim 2000^{\circ}\text{C}$ , $> \sim 15$ MPa [33, 34]<br>$\sim 1500^{\circ}\text{C}$ , $> \sim 2$ MPa [35], ( $\sim 0.1$ MPa [36]) |
| Metallic braze-based                             | Metallic fillers  | $\sim 1000^{\circ}\text{C}$ , low/no pressure [30, 37, 38]  |
| Glass ceramics                                   | Ca-Al-O<br>Si-Al-Mg-O<br>Y-Al-Si-O                                | $\sim 1500^{\circ}\text{C}$ , no pressure [39, 40]  |
| SiC pre-ceramics precursors                      | SiC   | $< \sim 1500^{\circ}\text{C}$ [41, 42], $\sim 0.01$ MPa [41]  |
| Reaction sintering with Si-C and Ti-Si-C systems | Si-C and Ti-Si-C  | $\leq \sim 1500^{\circ}\text{C}$ , [43-45] no pressure [43, 45]   |
| Liquid-phase sintering                           | SiC powder and sintering additives                                | $\sim 1850^{\circ}\text{C}$ , $\sim 10$ MPa [46-48]   |
| Selected area CVD/ CVI                           | SiC   | $< \sim 1200^{\circ}\text{C}$ , low pressure [18, 31]   |

### 2.5.1 Solid state diffusion bonding

Solid state self-diffusion bonding of SiC to SiC was demonstrated under hot-pressing at  $\sim 2000^{\circ}\text{C}$  under a pressure of  $> \sim 15$  MPa [33, 34]. This joining method allows interface-free joints as a result of thermally activated grain growth across the two bonded substrates. However, the dual requirements of applied stress and very high temperatures during the processing can limit the application of direct bonding to the end-plug joint. Moreover, direct bonding requires bonding faces with smooth surfaces and decent dimensional control to achieve adequate contact. These technical hurdles suggest another joining option—joining with an interlayer.

Solid state diffusion bonding with an interlayer typically uses a refractory metallic foil such as titanium, molybdenum, and tungsten [35]. The joining method is well established, and the advantage of this joining method is the relatively low joining temperature ( $\sim 1500^{\circ}\text{C}$ ). The drawback is the need for applied stress of more than a few MPa during the joining. Jung et al. recently overcame this limitation by solid state diffusion bonding using a titanium interlayer and added silicon powder and an applied stress of only  $\sim 0.1$  MPa [36], which makes this joining method attractive for the end-plug application.

### 2.5.2 Metallic braze-based joining

Brazing with various metallic filler materials has been widely studied for joining of SiC. For example, fillers of Ni-Cr-Si [37], Ag-Cu-Ti [38], and Al [30] systems were successfully applied to SiC-to-SiC plate joining and tube-end plug joining [30]. Brazing typically enables a relatively low processing temperature of  $\sim 1000^{\circ}\text{C}$  and low-pressure or pressureless joining. Since the filler material melts or softens during heating, applying the filler to components with complex geometries is relatively easy.

### 2.5.3 Glass ceramics joining

Glass ceramics bonding was demonstrated without applying external stress at relatively low temperatures ( $\sim 1500^{\circ}\text{C}$ ) for Ca-Al-O [40], Si-Al-Mg-O [40], and Y-Al-Si-O [39, 40] systems. The eutectic liquid or softened glass spreads across the joint plane, which enables good contact between the tube and end-cap without applied stress during joining.

### 2.5.4 Joining using SiC pre-ceramics precursors

This joining method provides an SiC-based joint layer at low processing temperatures ( $\leq \sim 1500^{\circ}\text{C}$ ) [41, 42]) and very low pressures ( $\sim 0.01$  MPa [41]). The common issue with this method is that large-volume shrinkage occurs during the pyrolysis of the precursors, which can cause cracking during the formation of the joint. The addition of SiC powder to the precursor increases the volumetric yield from the precursors and can mitigate issues associated with shrinkage. To form the joint, a bonding agent of a slurry consisting of an SiC forming polymer, an SiC powder, and a solvent may be applied to the joint plane by painting, followed by heating. A limitation of this method is the difficulty of obtaining a dense joint layer.

### 2.5.5 Reaction sintering with Si-C and Ti-Si-C systems

Reaction sintering or displacement reaction sintering is a method of fabricating ceramics using a powder feedstock; it is also used to join SiC materials. The Si-C [43] and Ti-Si-C [44, 45] systems are used for joining SiC plates. A slurry or green sheet containing the powder feedstock is applied to the bonding plane for joining. The processing temperature is relatively low ( $\leq \sim 1500^{\circ}\text{C}$  [43, 44]), and pressureless joining has been demonstrated for both reaction systems [43, 45].

### 2.5.6 Liquid-phase sintering of SiC

Liquid-phase sintering is a method widely used to fabricate dense SiC ceramics using SiC powder and sintering additives (typically oxides such as alumina-ytria) and is also an effective method of joining SiC materials [46-48]. The additives form a eutectic liquid during heating, and then the liquid phase promotes the sintering of an SiC powder compact via a solution-precipitation process [49]. The SiC powder mixture with a form of slurry or green tape is applied to the substrate for joining. The reported processing conditions are a maximum temperature of  $\sim 1850^{\circ}\text{C}$  and applied pressure of  $\sim 10$  MPa for the plate joints.

The key development for this joint type is a reduction of the joining pressure and control of the microstructure, especially for the secondary phases, for improved environmental resistance. The use of a nano-size SiC powder helped reduce the amount of sintering additives needed [50].

### **2.5.7 Selected-area chemical vapor deposition/infiltration**

Selected-area CVD or CVI of SiC provides a pure SiC bonding layer, which is expected to be very similar to the CVI matrix. Since this technique is limited to application on only one surface, a hybrid joining technique using SiC pre-ceramic joining followed by CVI SiC was proposed for end-plug applications [31].

### **2.5.8 Other methods**

In the case of an end-plug of NITE SiC/SiC composite cladding, a mechanical joint (screw type) was successfully applied because of the machinability of that composite [25]. A joint interlayer, as discussed in Section 2.5.1, may be applied to achieve adequate gas leak tightness.

## **3. NONIRRADIATED MATERIAL PROPERTIES**

### **3.1 Physical and Thermal Properties**

#### **3.1.1 Density, porosity, and fiber volume fraction**

The density of a typical CVI SiC/SiC composite flat specimen ranges from 2.3 to 2.7 g/cm<sup>3</sup> [6]. CVI SiC/SiC is less dense than NITE SiC/SiC [24]. For CVI SiC/SiC tubes, the theoretical density has been reported in the literature to be in the range of 80–88%. Considering that the density of fully dense SiC is 3.21 g/cm<sup>3</sup>, the range of density for CVI SiC/SiC tubes is 2.6–2.8 g/cm<sup>3</sup>. For NITE SiC/SiC composites, a 95% or higher theoretical density has been reported—about 2.96 g/cm<sup>3</sup> or higher. The porosity of CVI SiC/SiC composite tubes has been reported to be in the range of 8–17% [9, 51-53]. Less than 5% porosity has been reported [54] for NITE SiC/SiC composite tubes. Fiber volume fractions of 30–40% have been generally reported for CVI SiC/SiC composite tubes, with few exceptions. The fiber volume fraction directly affects the strength of the material: the higher the fiber volume fraction, the higher the strength of the material [9]. Table 4 summarizes the physical properties of various types of SiC/SiC tubes.

Table 4. Summary of different SiC/SiC tubes and their physical properties

| Matrix  | Fiber            | Interphase | Type                         | Fiber architecture                         | Density [g/cm <sup>3</sup> ] | Fiber volume fraction [%] | Porosity [%] | Outer diameter [mm] | Wall thickness [mm] | Reference |
|---|------------------|------------|------------------------------|--|------------------------------|---------------------------|--------------|---------------------|---------------------|-----------|
| <b>Unknown Manufacturers</b>  |                  |            |                              |  |                              |                           |              |                     |                     |           |
| CVI   | HNS              | 100 nm PyC | Full SiC/SiC                 | Three layers $\pm 45^\circ$ from tube axis | <i>a</i>                     |                           | 10.4–11.1    | 9.6                 | 1.75                | [51]      |
| CVI   | HNS              | Carbon     | Triplex/monolith-SiC/SiC-CVI |  |                              |                           |              | ~10                 |                     | [55]      |
| CVI   | IBN              | Carbon     | Triplex/monolith-SiC/SiC-CVI |  |                              |                           |              | ~10                 |                     | [55]      |
| NITE  | SAK <sup>b</sup> | PyC        | Full SiC/SiC                 |  |                              |                           |              |                     |                     | [56]      |
| Similar to NITE   | SA3              | 200 nm PyC | Full SiC/SiC                 |  |                              |                           | ~5           |                     |                     | [57]      |
| <b>CEA (French Alternative Energies and Atomic Energy Commission)</b> |                  |            |                              |  |                              |                           |              |                     |                     |           |
| CVI   | HNS              | PyC        | Full SiC/SiC                 | $\pm 30^\circ$ along tube axis             |                              | 35                        |              | 9.6                 | 1.7                 | [58]      |
| <b>Ceramic Tubular Products, LLC</b>                                  |                  |            |                              |  |                              |                           |              |                     |                     |           |
| CVI   | HNS              |            | Duplex                       |  |                              |                           |              |                     | ~0.75               | [8]       |
| CVI   | HNS              |            | Triplex/monolith-SiC/SiC-CVI |  |                              |                           |              |                     | ~0.75               | [8]       |
| CVI   | IBN              |            | Triplex/TREX-SiC/SiC-CVI     |  |                              |                           |              |                     | ~0.75               | [8]       |

Table 4. Summary of different SiC/SiC tubes and their physical properties (continued)

| Matrix  | Fiber          | Interphase    | Type                   | Fiber architecture  | Density<br>[g/cm <sup>3</sup> ] | Fiber<br>volume<br>fraction<br>[%] | Porosity<br>[%]                       | Outer<br>diameter<br>[mm] | Wall<br>thickness<br>[mm] | Reference |
|---|----------------|---------------|------------------------|---|---------------------------------|------------------------------------|---------------------------------------|---------------------------|---------------------------|-----------|
| <b>General Atomic</b>                         |                |               |                        |   |                                 |                                    |                                       |                           |                           |           |
| CVI   | HNS            | PyC           |                        |   |                                 | 30–35                              | ~12                                   | 10.63                     | 1.4                       | [59]      |
| CVI   | HNS            | 150 nm<br>PyC | Duplex                 | Axial biased (1.5<br>axial: 1 hoop)<br>Hoop biased, ±45°<br>(1:1) |                                 |                                    | ~20                                   | 8.8–9.6                   | 1.2–2.1                   | [7]       |
| CVI   |                |               | Full SiC/SiC<br>duplex |   |                                 | 35                                 | 12.7<br>8.7                           | 10                        | 1.8                       | [52]      |
| CVI   | HNS            | PyC           | Full SiC/SiC           | ±55° from tube<br>axis with axial<br>reinforcement                | 2.6–2.8                         | 51                                 | ~13.75                                | ~9.5                      | ~0.78                     | [53]      |
| <b>Korea Atomic Energy Research Institute</b> |                |               |                        |   |                                 |                                    |                                       |                           |                           |           |
| CVI   | HNS and<br>SA3 | 200 nm<br>PyC | Triplex                | ±45°, 55°, 65°  |                                 | 18–25                              | 10–17%<br>for CVI<br>SiC/SiC<br>layer | 9.6–10.1                  | 1.1–1.6                   | [9]       |
| <b>Muroran Institute of Technology</b>        |                |               |                        |   |                                 |                                    |                                       |                           |                           |           |
| NITE  |                | PyC           | Full SiC/SiC           | ±60° from tube<br>axis  |                                 |                                    |                                       | 10                        | 1                         | [54]      |
| NITE  |                |               | Full SiC/SiC           |   |                                 |                                    | <~5%                                  | 12                        | 2                         | [54]      |

<sup>a</sup> Empty cell information is not currently available.

<sup>b</sup> The new version of Tyranno SA fiber.

### 3.1.2 Thermal expansion

The coefficient of thermal expansion (CTE) of SiC/SiC tubes is rarely reported so far. However, it is expected that the CTEs of the tubes are similar to those of plate materials because of the similarity of the microstructures. Previous work [6] reported that the instantaneous CTE of CVI SiC/SiC composite plates followed Eq. (1) regardless of the fiber type (HNS or SA3).

$$\alpha (10^{-6}/K) = -0.7765 + 1.4350 \times 10^{-2}T - 1.2209 \times 10^{-5}T^2 + 3.8289 \times 10^{-9}T^3, (293K < T < 1273K) \quad (1)$$

where  $\alpha$  and  $T$  indicate CTE and temperature, respectively. This study also confirms that Eq. (1) is applicable to CVI SiC/SiC composite plates neutron irradiated under LWR-relevant temperature and dose conditions (as is discussed later in this report).

For the CTEs of NITE SiC/SiC composites, the data are rare even for a plate specimen. The CTEs of NITE SiC/SiC composites may be assumed to be similar to those of CVI SiC/SiC composites, according to the insignificant effects of oxide phases on the CTEs of monolithic SiC [60].

### 3.1.3 Thermal diffusivity

The thermal diffusivity of the cladding is a key property characterizing the capability for heat transfer from fuel to coolant. A higher thermal diffusivity results in a lower fuel temperature and smaller through-thickness temperature gradient of the cladding. Therefore, higher thermal diffusivity is usually beneficial for cladding applications.

The thermal diffusivity of SiC/SiC tubes along the wall thickness was evaluated by a laser flash method using a curved square section machined from an SiC/SiC tube [52]. The reported thermal diffusivities are listed in Table 5. Although the measurement method has not yet become a test method standard, the values appeared to be reasonable based on the results from plate specimens [6]. The results showed that triplex SiC/SiC tubes exhibited higher thermal diffusivity than duplex and full composite tubes because of the higher diffusivity of the monolithic layer compared with the composite layer. There are no data available for the in-plate thermal diffusivity of SiC/SiC tubes because of difficulty of measurement. It is expected that the in-plane diffusivity is higher than the through-thickness diffusivity, according to the results from plate specimens [6]. It is clear that a standard test method for ceramics tubes is needed. Until a standard method is available, thermal diffusivity measurements obtained from plate specimens [6] may be used for modeling purposes.

Table 5. Through-thickness thermal diffusivity of CVI SiC/SiC tubes evaluated using a laser flash method

| Material  | Room temperature<br>[mm <sup>2</sup> /s] | 300°C<br>[mm <sup>2</sup> /s] | 800°C<br>[mm <sup>2</sup> /s] | Reference |
|---|--|-------------------------------|-------------------------------|-----------|
| Duplex SiC/SiC composite with 150 nm PyC coated NHS fiber reinforcement | 8~9                                      | 4.5~5.5                       | 4~4.5                         | [7]       |
| Full SiC/SiC composite<br>(no information on fiber type)                | 2~7                                      | 1.25~4.5                      | 1~3.25                        | [52]      |
| Duplex SiC/SiC composite<br>(no information on fiber type)              | 8.5~13                                   | 5~7.5                         | 3~5                           | [52]      |
| Triplex SiC/SiC composite with HNS fiber<br>(no interphase information) | ~25                                      | ~13                           | No data                       | [8]       |



### 3.1.4 Specific heat

The specific heat of SiC/SiC tubes has not been reported so far. However, the value can be expected to be almost the same as that for SiC/SiC plates. The specific heat of SiC/SiC plates is considered to be the same as that of monolithic SiC (high-purity SiC) because of the negligible effect of the presence of a carbon interphase [6]. The temperature-dependent specific heat of monolithic SiC materials was reported in Snead et al. 2007 [61] (Figure 3).

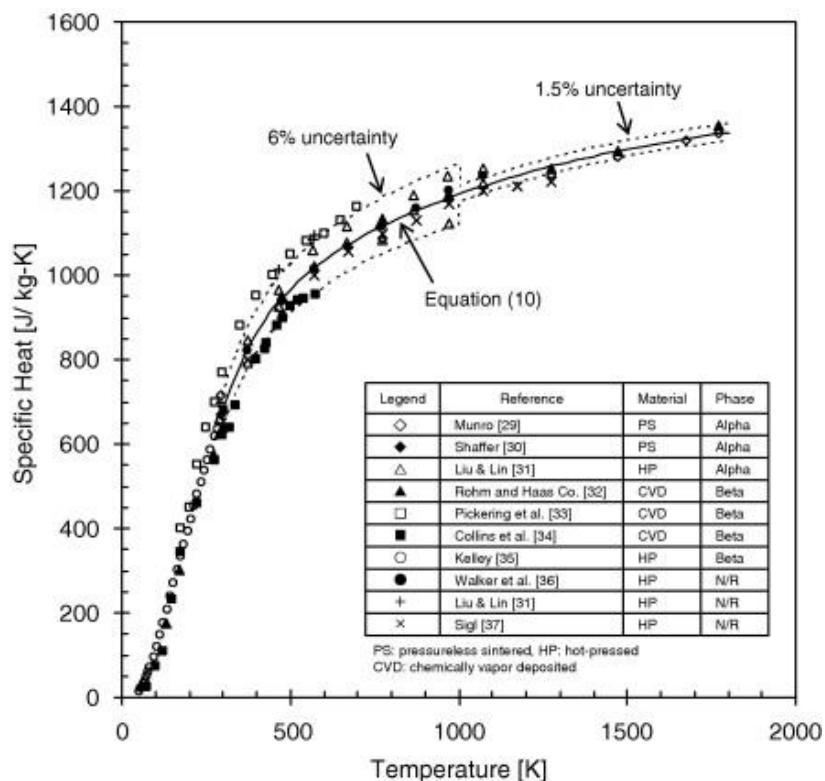


Figure 3. Specific heat of SiC at elevated temperatures [61].

### 3.1.5 Gas leak tightness

One of the primary functions of the cladding itself is to maintain an impermeable barrier to prevent fission gas release from the fuel into the reactor primary coolant. A criterion of SiC/SiC composite tube failure is a loss of gas tightness. Any increase in the extent of fission gas release from the fuel will be directly proportional to the increase in the radioactivity in the primary coolant and the fission gas (e.g., tritium) release to the environment. Moreover, helium is used as the heat conduction medium between the fuel and the cladding. A loss of hermeticity (an indication of the gas leak tightness) would lead to the release of helium. As a consequence, the heat produced in the fuel could not be efficiently removed and the probability of fuel failure would increase. Therefore, the hermeticity of the SiC-based cladding needs to be assessed.

This section discusses the gas permeability of SiC and the gas leakage rate of an SiC/SiC cladding system. Permeability, an intrinsic physical property of a continuous solid, is expressed as a product of gas solubility and diffusivity. The gas leakage rate is a measure of the effectiveness of the seal of the material or system, as indicated by the flux of gas that passes through the leak.

### 3.1.5.1 Permeability

Assuming 1D transport, the flux,  $J$ , of gas permeating through the sample can be derived from Fick's first law, assuming gas solubility governed by Sieverts' law. It is given by

$$J = \frac{DS(P_i^{1/2} - P_o^{1/2})}{\delta}, \quad (2)$$

where  $\delta$  is the clad wall thickness of the sample, and  $P_i$  and  $P_o$  are the gas pressures in the upstream and downstream chambers, respectively.  $P_o$  is negligible if the downstream chamber is always under an ultra-high vacuum ( $\sim 1 \times 10^{-7}$  torr) during measurement. The product of diffusivity,  $D$ , and Sievert's parameter,  $S$ , (note that  $S$  is usually defined as "solubility" in gas permeation studies) is defined as the permeability,  $\Phi$ , which can be expressed in the form of

$$\phi = DS = \frac{J\delta}{P_i^{1/2}}, \quad (3)$$

Units used here for  $D$  and  $S$  are, respectively,  $m^2/s$  and  $mol H_2 m^{-3} MPa^{-1/2}$ , giving rise to the unit  $\Phi$ ,  $mol H_2 m^{-1} s^{-1} MPa^{-1/2}$ . Therefore, measurement of the permeation flux will result in the determination of permeability. For most materials, permeability follows the Arrhenius temperature dependence. Thus, it can be expressed as

$$\phi = \phi_0 \exp\left(-\frac{E}{RT}\right), \quad (4)$$

where  $\Phi_0$  is the permeability constant and  $E$  is an apparent activation energy for permeation (essentially the sum of activation energies for dissolution and diffusion). Measurements of the permeability at various temperatures will enable the determination of  $E$  and  $\Phi_0$ .

Various results for the permeation of hydrogen isotopes in SiC have been reported by different authors. An issue in previous efforts has been that most of the work did not show material qualities such as purity and grain size, although different grades of SiC showed significantly different permeabilities. Regardless of the SiC material quality, SiC is considered a good permeation barrier compared with metallic materials. Yamamoto et al. [62] report the deuterium permeation of CVD SiC fabricated by Rohm and Haas (currently Dow Chemical). The microstructural features of this material exhibited almost full density, a purity of >99.9995%, an average grain size of  $\sim 5 \mu m$ , limited grain texture, and the presence of the stacking faults within the grains [63]. The permeation behavior is described by [62] at 600–950°C [62].

$$\Phi = 130 \exp(-230kJ/RT) \text{ mol s}^{-1} \text{ m}^{-1} \text{ MPa}^{-1/2}. \quad (5)$$

This result shows that CVD SiC-coated SiC-based cladding is considered gastight in the absence of processing defects.

### 3.1.5.2 Gas leakage rate

Based on the requirements for the current Zr cladding system, it is reported that a helium leakage rate should be no greater than  $1 \times 10^{-6}$  mbar l  $s^{-1}$  at 17 bar and room temperature for an entire 14 foot fuel rod

[31]. Table 6 summarizes the gas leakage rate of CVI and NITE SiC/SiC tubes. Hermetic tubes for both types of materials have been achieved.

Table 6. Gas leakage rate for SiC/SiC tubes

| Material  | Specimen geometry [mm]  | Test condition   | Gas leak rate   | Reference |
|---|---|--|---|-----------|
| CVI SiC/SiC tube with SiC end-plug                    | ID ~7.5<br>Wall thickness 1.2-2.1                                       | Gas: He<br>$\Delta P = 0.1 \text{ MPa}$ @ room temperature   | $< 1.01 \times 10^{-13} \text{ Pa m}^3/\text{s}$  | [7]       |
|   |   | Gas: He<br>$\Delta P = 0.1 \text{ MPa}$ @ 300°C (after 1000°C thermal cycle and 16.8 MPa applied gas pressure) | $4.1 \times 10^{-10} \text{ Pa m}^3/\text{s}$   |           |
| CVI SiC/SiC tube coated with CrN or TiN and open ends | Length 16<br>ID 7.1<br>Wall thickness 1.4                               | Gas: He and D <sub>2</sub><br>$\Delta P \leq \sim 0.1 \text{ MPa}$ @ room temperature                          | $< 1.01 \times 10^{-13} \text{ Pa m}^3/\text{s}$ for both He and D <sub>2</sub>   | [64]      |
| NITE SiC/SiC tube with open ends                      | Length 200<br>ID 10<br>Wall thickness 1 (uniform heating length, 30 mm) | Gas: He and H <sub>2</sub><br>$\Delta P < 0.01 \text{ MPa}$  | He $< 2 \times 10^{-12} \text{ Pa m}^3/\text{s}$ up to 400°C<br>H <sub>2</sub> $< 1 \times 10^{-8} \text{ Pa m}^3/\text{s}$ up to 400°C | [54]      |

## 3.2 Mechanical Properties

Properties related to mechanical failure include the stresses for the first major matrix cracking, the first penetrating crack formation, and ultimate failure. Statistical factors for these properties are insufficiently understood for nuclear-grade SiC/SiC composite tubes. The statistical factors include both the governing statistic laws and statistical parameters such as Weibull parameters. These are especially important at the extremes of the failure distribution. Part of the focus of this section is the mechanical properties dependence on the fiber reinforcement angle. This dependence has been reported in both filament-wound and 2D braided CVI SiC/SiC tubes, although a detailed analysis was not provided [12].

### 3.2.1 Young's modulus

The typical in-plane Young's modulus for nuclear-grade CVI SiC/SiC composite planar specimens has been reported to be in the range of 200–280 GPa [6].

Compared with planar specimens, fewer studies have been conducted for tubular SiC/SiC composites, and Young's moduli, mostly from tensile tests, are available in the literature. The reported Young's moduli for axial tensile tests lie in the range of 200–250 GPa [7, 51, 53, 58]; and for hoop tensile tests, one study [58] has reported the value of Young's modulus to be 158 GPa. One study has reported the Young's modulus under compression: 251 GPa [51].

For tube specimens, the coefficient of variance (C.V.) for Young's modulus has been reported to be mainly in the range of 7–20% [7, 51, 53, 58]. A round-robin study [53] showed a significant variation in C.V. across the laboratories, indicating a strong dependence on the material, operator, and test equipment of the spread in the modulus data.

Shear modulus value ranging from 80–120 GPa have been reported for flat specimens [6]. Those values were calculated from the Young's modulus and Poisson's ratios. Only one study reported the shear modulus for tube specimens [53]. Figure 4 shows the Young's modulus determined from various studies

of tubes. The linear fit line indicates a moderate effect of fiber winding angle on the axial Young's modulus of SiC/SiC tubes.

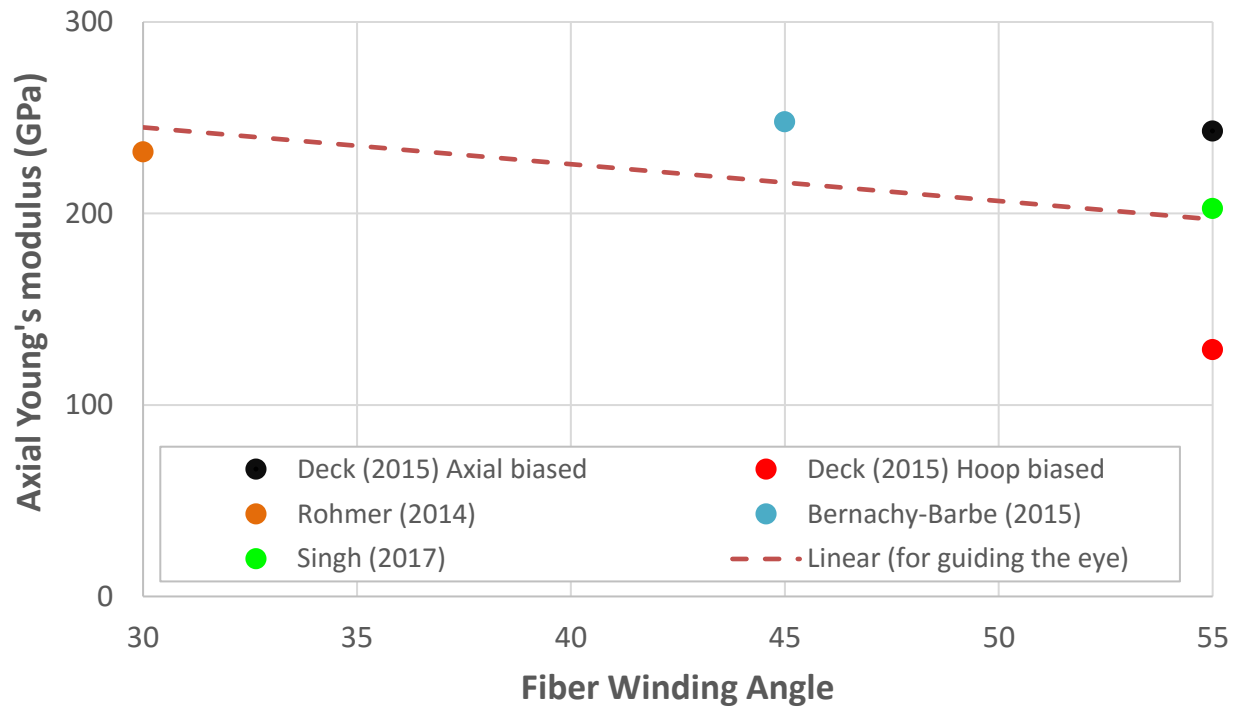


Figure 4. Axial Young's moduli determined from several studies for CVI SiC/SiC tubes.

Table 7 summarizes the tensile and hoop mechanical behavior of the SiC/SiC tube specimens.

Table 7. Compilation of mechanical properties of SiC/SiC composite determined from tests on tube specimens

| Material                                   | Loading<br>(Test method)   | Young's<br>modulus<br>(GPa) | PLS<br>(MPa)   | UTS<br>(MPa)                 | Strain at<br>PLS<br>(%) | Strain at<br>UTS<br>(%) | Shear<br>strength<br>(MPa) | Number<br>of test | Fiber architecture/<br>porosity/fiber volume<br>fraction                   | Ref. |
|--|--|-----------------------------|--|------------------------------|-------------------------|-------------------------|----------------------------|-------------------|--|------|
| CVI, HNLS<br>100 nm PyC                    | Uniaxial tension<br>(Monotonic axial<br>tensile test)            | 248 (14)                    | ~100   | 269                          | ~1                      |                         |                            | 3                 | ±45°, inner layer filament<br>wound, outer layers 2×2<br>braids/10.4–11.1% | [51] |
|  | Uniaxial<br>compression<br>(Monotonic axial<br>compression test) | 251 (15)                    | ~130   | 385                          |                         |                         |                            | 3                 |  |      |
|  | Hoop tension<br>(Internal<br>pressurization)                     |                             |  | 303                          |                         |                         |                            | 3                 |  |      |
|  | Equibiaxial<br>(tension, internal<br>pressurization)             |                             |  | 297                          |                         |                         |                            | 2                 |  |      |
|  | Pure torsion   |                             |  |                              |                         |                         | 286                        |                   |  |      |
| Full SiC/SiC<br>axial biased <sup>1</sup>  | Hoop tension<br>(C-ring)   |                             |  | 209 (24)                     |                         |                         |                            |                   | ±~50~60°/~20%/-  | [7]  |
| Full SiC/SiC<br>hoop biased <sup>2</sup>   | Hoop tension<br>(C-ring)   |                             |  | 331 (74)                     |                         |                         |                            |                   |  |      |
| Full SiC/SiC,<br>axial biased <sup>1</sup> | Uniaxial tension<br>(Monotonic axial<br>tensile test)            | 243 (19)                    |  | 236 (35)                     |                         |                         |                            |                   |  |      |
| Full SiC/SiC<br>hoop biased <sup>2</sup>   | Uniaxial tension<br>(Monotonic axial<br>tensile test)            | 129 (14)                    |  | 93 (14)                      |                         |                         |                            |                   |  |      |
| Duplex: Monolith<br>(inside) and SiC/SiC   | Hoop tension<br>(C-ring)   |                             |  | 174 (28), <sup>3</sup> m=7.0 |                         |                         |                            |                   |  |      |
| Full SiC/SiC                               | Hoop tension<br>(C-ring)   |                             |  | 209 (24), m=7.9              |                         |                         |                            |                   |  |      |
| Duplex: Monolith<br>(outside) and SiC/SiC  | Hoop tension<br>(C-ring)   |                             |  | 311 (59), m=4.6              |                         |                         |                            |                   |  |      |
| Full SiC/SiC                               | Hoop tension<br>(C-ring)   |                             |  | 304 (14), m=12.1             |                         |                         |                            |                   |  |      |
| Duplex: Monolith<br>(inside) and SiC/SiC   | Hoop tension<br>(expanding plug)                                 | 278 (20)                    | <sup>4</sup> OD: 92 (6),<br><sup>5</sup> ID: 140 (7) | OD: 152 (8)<br>ID: 231 (9)   |                         |                         |                            |                   |  |      |
| Duplex: Monolith<br>(outside) and SiC/SiC  | Hoop tension<br>(expanding plug)                                 | 288 (13)                    | OD: 129 (10)<br>ID: 158 (12)                         | OD: 271 (2),<br>ID: 332 (3)  |                         |                         |                            |                   |  |      |

| Material  | Loading<br>(Test method)                           | Young's<br>modulus<br>(GPa) | PLS<br>(MPa)   | UTS<br>(MPa)             | Strain at<br>PLS<br>(%) | Strain at<br>UTS<br>(%) | Shear<br>strength<br>(MPa) | Number<br>of test | Fiber architecture/<br>porosity/fiber volume<br>fraction               | Ref. |
|---|--|-----------------------------|--|--------------------------|-------------------------|-------------------------|----------------------------|-------------------|--|------|
| Triplex: CVI SiC/SiC<br>at middle, monolith<br>outside and inside,<br>200 nm PyC (SA3,<br>HNLS) | Hoop tension<br>(internal<br>pressurization)       |                             |  | 282.4 (44.3);<br>m=11.05 |                         |                         |                            |                   | See Section 3.2.2, $\pm 45^\circ$ ,<br>$\pm 55^\circ$ , $\pm 65^\circ$ | [9]  |
| CVI SiC/SiC, HNLS   | Axial tension<br>(monotonic axial<br>tensile test) | 232.2 (17.1)                | 82.75 (12.76)  | 462.7 (37.3)             | 0.034<br>(0.007)        | 0.685<br>(0.087)        |                            | 4                 | $\pm 30^\circ$ / - /35%  | [58] |
| CVI SiC/SiC, HNLS   | Hoop tension<br>(internal<br>pressurization)       | 157.5 (27.6)                | 35.5 (6.36)  | 63 (0.7)                 | 0.032<br>(0.015)        | 1.51<br>(0.014)         |                            | 2                 |  |      |
| CVI SiC/SiC, HNLS,<br>150nm PyC   | Axial tension<br>(monotonic axial<br>tensile test) | 202.7 (40.3)                | 92.6 (9.0), log<br>mean: 4.52, log<br>standard<br>deviation: 0.096 | 236.8 (29.6),<br>m=10.1  | 0.057<br>(0.007)        | 0.53<br>(0.1)           |                            | 43                | $\pm 55^\circ$ with axial<br>reinforcement/14%/51%                     | [53] |

Notes:

Number of test:

1 Fiber reinforcement ratio (hoop: axial) 1: 1.5

2 Fiber reinforcement ratio (hoop: axial) 1.3: 1

3 Weibull modulus

4: Outer diameter

5: Inner diameter

Values in brackets are standard deviation.

### 3.2.2 Proportional limit stress

For flat specimens, the proportional limit stress (PLS) has most frequently been reported in the 90–120 MPa range [6]. For tube specimens, axial PLS has been generally reported between 80 and 100 MPa [51, 53, 58]. In the hoop direction, relatively higher PLS values have been reported [7], ranging from 100 MPa to 160 MPa. Bernachy-Barbe et al. [51] report axial PLS of about 130 MPa under compression, which is slightly greater than the reported PLS under tension (about 100 MPa). Most studies report a standard deviation of 10 MPa or less [51]. Singh et al. [53] has reported that PLS follows log-normal distribution with the log-mean and log-standard deviation of 4.52 and 0.096.

Fiber architecture greatly influences the PLS. Nozawa et al. [65] has systematically shown the effect of fiber orientation on mechanical properties in flat specimens; PLS decreases by over 25% when the fiber orientation is changed from  $0^\circ/90^\circ$  to  $\pm 45^\circ$ . Tests conducted by Rohmer et al. [58] on tube specimens with  $\pm 30^\circ$  fiber orientation led to a PLS of 36 MPa in the hoop direction and 83 MPa in the axial direction.

### 3.2.3 Ultimate tensile strength

An in-plane UTS of 250–350 MPa has been generally reported for flat specimens. However, for tube specimens, UTS has been measured as being in the range of 230–270 MPa in the axial direction and 200–340 MPa in the hoop direction in most studies. The strength values reported toward the higher end of this range are for specimens having a fiber fraction biased in the hoop direction [7]. The typical C.V. for UTS for tube specimens ranged between 10 and 20 %, although C.V.s outside this range have been also reported.

There is a significant effect of fiber orientation on the UTS. Nozawa et al. [65] measured a decrease in UTS (failure stress) of about 35% upon changing the fiber orientation by  $45^\circ$  in flat specimens. Rohmer et al. [58] reported a significantly smaller hoop strength (63 MPa) than the axial strength (463 MPa) for tube specimens with a  $\pm 30^\circ$  fiber orientation with regard to the tube axis. Kim et al. [9] tested triplex SiC tube specimens and showed an increase in the hoop strength by over 15% after an increase in the fiber orientation from  $\pm 45^\circ$  to  $\pm 65^\circ$  for SiC triplex tubes. The hoop strength of the specimens ranged from 235 to 338 MPa. In the Kim et al. study, tubes with Tyranno SA3 fibers exhibited greater strength than tubes with HNS fibers; the study also shows that the fiber winding method influences the strength significantly.

Figure 5 and Figure 6 show the axial and hoop UTS determined from various studies involving SiC/SiC tube specimens. The steep slope of the linear fit indicates a significant effect of the fiber winding angle on UTS.

Studies have reported Weibull moduli range of 7-12 for UTS [7, 9, 53]. Singh et al. [53] has shown that UTS data fit best with Weibull distribution.

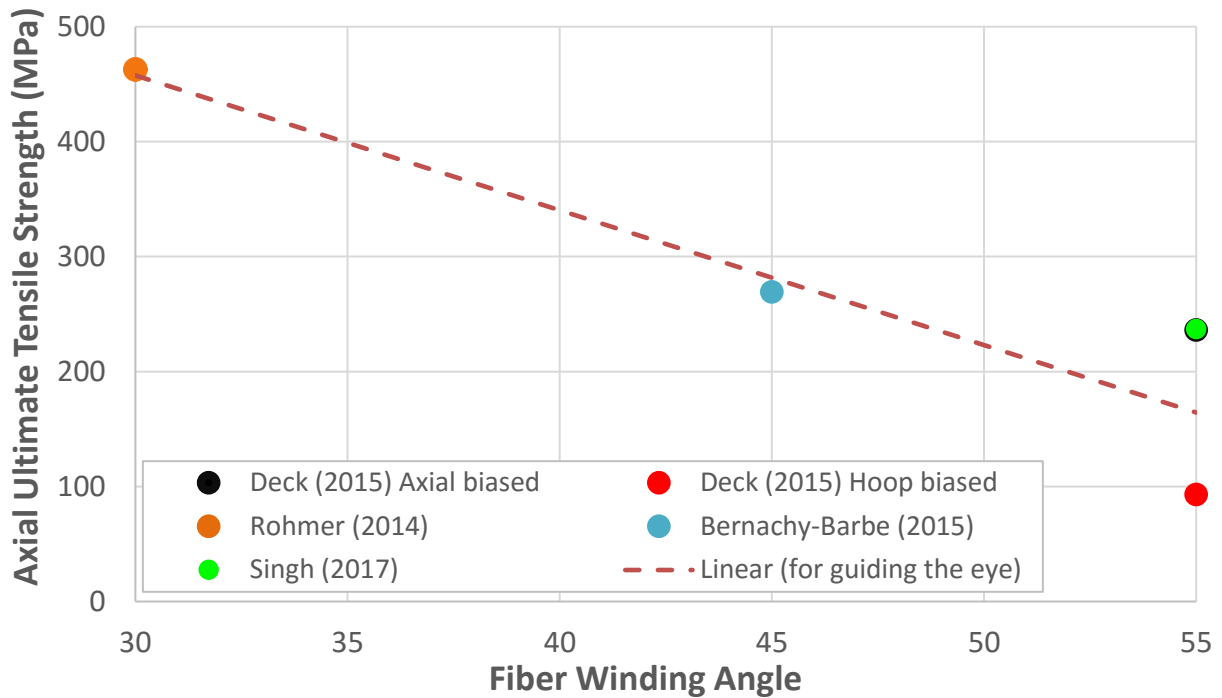


Figure 5. Axial UTS determined from several studies for CVI SiC/SiC tubes.

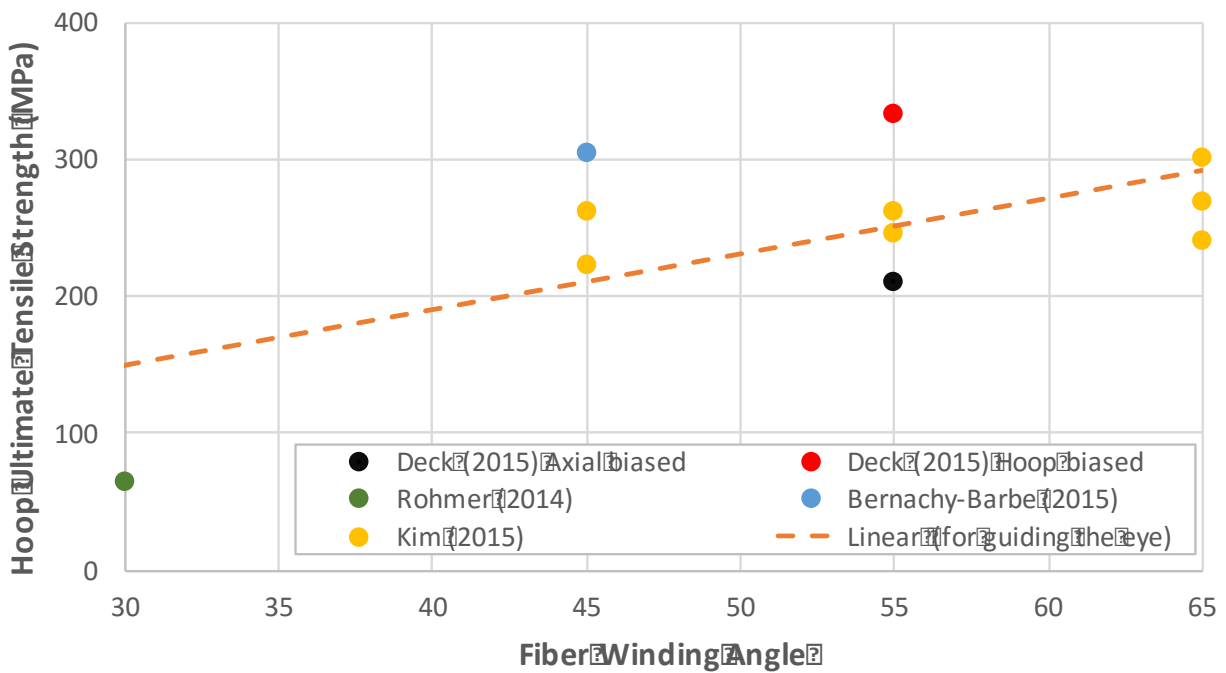


Figure 6. Hoop UTS determined from several studies for CVI SiC/SiC tubes.



### 3.2.4 Strain at proportional limit strength and ultimate tensile strength

The strain at PLS has been measured to be in the range of 0.03–0.06% for studies involving tubes. Strain at UTS has been reported to range from 0.6 to 0.85%. The C.V.s for strains at PLS and UTS range from 10 to 20% for most studies on tubes [53, 58]

### 3.2.5 Poisson's Ratio

Nozawa et al. [65] report the in-plane Poisson's ratios for plate specimens oriented at different angles from the direction of loading. The reported data show that when the fiber orientation with loading was changed from 0°/90° to ±45°, the Poisson's ratio increased from ~0.13 to ~0.25 for plain-weave CVI and NITE SiC/SiC composites under tensile as well as compressive tests. There is no data on Poisson's ratio from tube studies.

## 3.3 Corrosion, Oxidation and Fuel Compatibility

### 3.3.1 Hydrothermal corrosion

SiC recession as a result of corrosion in high-temperature water leads to (1) cladding thickness losses that could in turn result in increased loading on the structure and (2) deposition of unwelcome corrosion products in the primary water circuit. Therefore, it is essential to quantify the rate of SiC recession, along with its dependence on environmental conditions such as pH, oxygen potential, electrochemical potential, solutes in the aqueous systems, and radiolysis. This section discusses the corrosion behavior of SiC materials and candidate EBC materials in simulated reactor coolant without considering irradiation effects such as displacement damage and radiolysis.

#### 3.3.1.1 Corrosion of SiC matrix

In the case of a cladding design without a non-SiC EBC, the SiC matrix is expected to be the first barrier against the coolant water, and no fiber and carbon interphase are expected to be exposed. Figure 7 summarizes the hydrothermal corrosion behavior of monolithic high-purity CVD SiC. It corresponds to the matrix of a CVI SiC/SiC composite in a simulated reactor coolant environment, including pressurized water reactor (PWR), boiling water reactor (BWR) hydrogen water chemistry (HWC), and BWR normal water chemistry (NWC), all without irradiation [66, 67]. Figure 7 clearly shows that different water chemistries lead to different corrosion behaviors. The previous corrosion study highlighted that the dissolved oxygen activity in water greatly increased SiC recession. Not only the water chemistry, but also material qualities such as grain size and grain texture, likely affect the corrosion resistance, since preferential attack at the grain boundary has been reported [66, 67]. In fuel cladding applications, depending on the in-pile recession kinetics of SiC and the thickness of the matrix on the surface, a loss of cladding thickness can potentially expose the fiber-matrix interphase. This exposure can lead to damage to the fiber and/or interphase and consequently degrade the composite's mechanical properties.

The kinetics of SiC recession under hot water is governed by a surface oxidation reaction (silica formation), because once silica forms on SiC under hydrothermal conditions, it readily dissolves in water. Therefore, it is also important to consider that the silica concentration in the reactor coolant can reach the point of saturation, and then the silica will deposit in the relatively cold regions of the coolant loop [66]. It is doubtful that significant amounts of deposited silica in the reactor core can be allowed during operation.

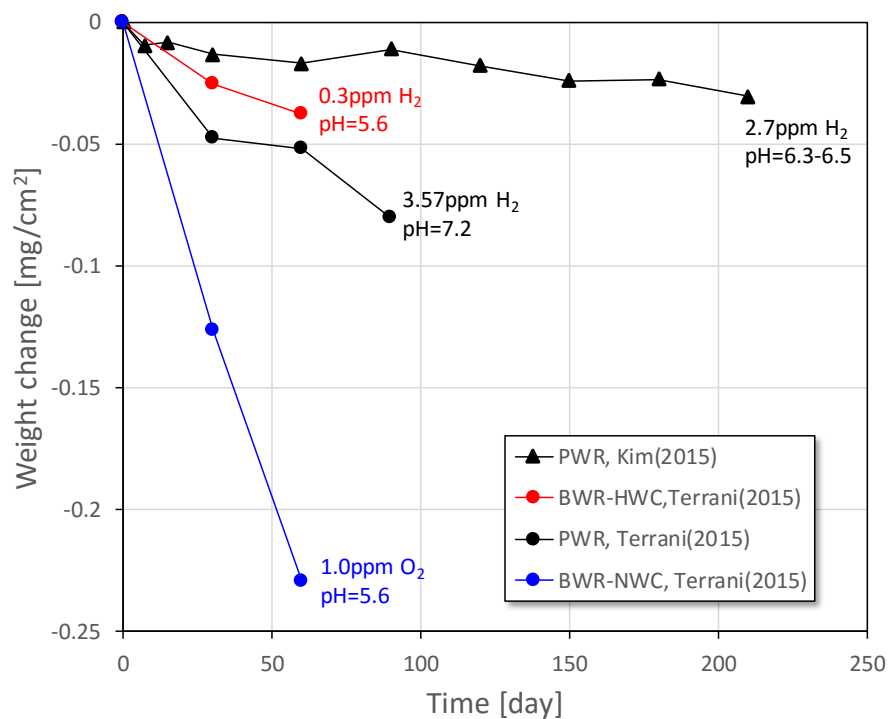


Figure 7. Mass change in CVD SiC after exposure to simulated reactor water loops [66, 67]. The temperature and pressure ranged from 290 to 360°C and 7–20 MPa, respectively, depending on the water chemistry.

For NITE SiC/SiC composites, a systematic investigation of the hydrothermal corrosion behavior of the matrix has not been reported. However, the corrosion behavior has been investigated for monolithic SiC ceramics. Their microstructure was found to be similar to that of the NITE matrix: a relatively small grain size (submicron to a few microns) and the presence of oxide secondary phases along the grain boundaries (as a thin film a few nm in width) and at grain pockets. These monolithic SiC ceramics are referred to NITE ceramics in this paper for convenience. Parish et al. report the recession of NITE SiC ceramics with three different additive systems under the simulated PWR, BWR-HWC, and BWR-NWC coolant environments without irradiation, as shown in Figure 8 [26]. The recession rates of NITE SiC ceramics were more than one order higher than those of CVD SiC specimens; the poor corrosion resistance was attributed to the secondary phases preferentially attacked under hydrothermal conditions. This work also demonstrated that corrosion properties can be improved by controlling secondary phases. At the time of the current report, hydrothermal corrosion-resistant NITE SiC/SiC composites have not yet been demonstrated. An EBC on the clad surface may be an option for NITE SiC/SiC cladding.

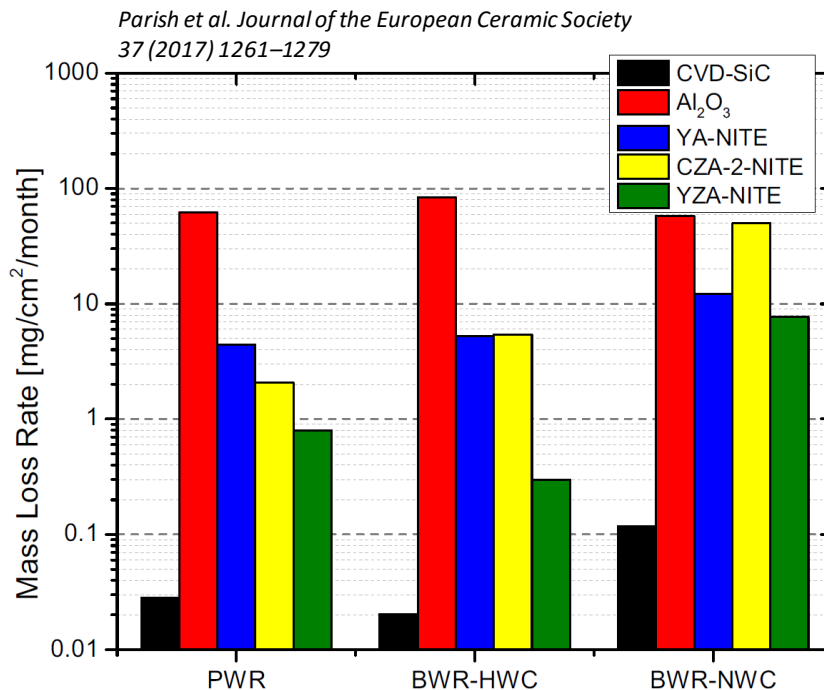
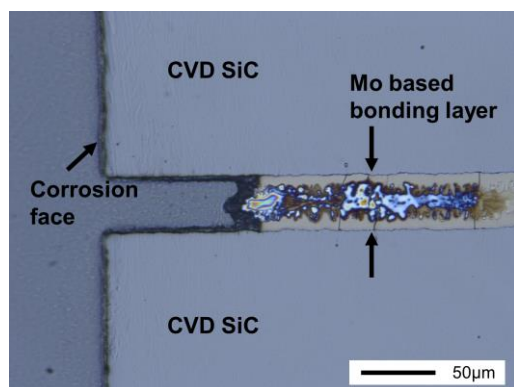


Figure 8. Linear mass loss rate for NITE SiC with various sintering additives, CVD-SiC, and polycrystalline alumina [26]. The corrosion test was conducted for up to 3 months for CVD SiC, 2 months for YA-NITE, and 5 weeks for the other materials. YA-NITE, CZA-2-NITE, and YZA-NITE are NITE ceramics fabricated with sintering additives of Y<sub>2</sub>O<sub>3</sub>-Al<sub>2</sub>O<sub>3</sub>, CeO<sub>2</sub>-ZrO<sub>2</sub>-Al<sub>2</sub>O<sub>3</sub>, and Y<sub>2</sub>O<sub>3</sub>-ZrO<sub>2</sub>-Al<sub>2</sub>O<sub>3</sub> systems, respectively.

### 3.3.1.2 Corrosion of SiC joint

Hydrothermal corrosion of the end-plug joint is also considered a feasibility issue. The allowable recession rate may depend on the joint geometry; a larger bonding area provides more allowance for recession. Koyanagi et al. report the hydrothermal corrosion behavior of various SiC-to-SiC plate joints under simulated reactor coolant environments for 5 weeks [45]. The tested joints include a molybdenum diffusion bond, a titanium diffusion bond, a Ti-Si-C reaction sintered bond, and an SiC nanopowder sintered bond. Under a reducing activity environment (PWR and BWR-HWC), only the molybdenum diffusion bond showed poor corrosion resistance (Figure 9a). However, under a BWR-NWC oxidizing activity environment, all of the joints except the SiC nanopowder sintered joint experienced significant recession. The sintered SiC joint exhibited only a 5 micron recession relative to the CVD SiC substrate following corrosion testing for 5 weeks (Figure 9b). Another promising joint was a selected-area CVD or CVI SiC joint that forms a high-purity SiC bonding layer.

(a) Mo diffusion bond tested with BWR-HWC for five weeks



(b) Nano-powder sintered SiC joint tested with BWR-NWC for five weeks

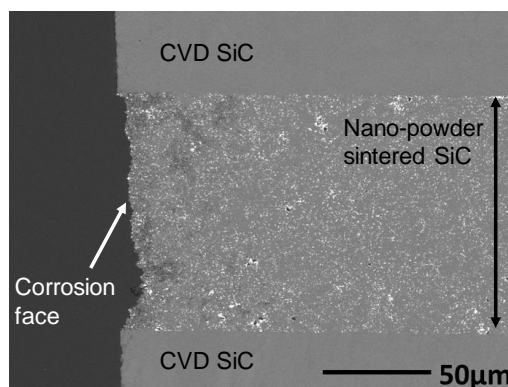


Figure 9. Cross-sectional observation of SiC joints after autoclave immersion: (a) molybdenum diffusion bond tested with BWR-HWC for 5 weeks and (b) nanopowder sintered SiC joint tested with BWR-NWC for 5 weeks [45].

### 3.3.1.3 Corrosion of coating

An EBC on the outer surface of the cladding will be required if SiC composites undergo unacceptable recession in the coolant. Several types of corrosion-resistant EBCs are under development for Zr-based claddings [27]. The corrosion-resistant coating materials applicable for SiC include chromium-based (chromium [68-70] and CrN), titanium-based (TiN/Ti layer [71, 72] and TiAlN [73]), and iron-based materials (FeCrAl alloy [74]). The reported corrosion resistance of each of these coatings is summarized in Table 8. All of the coating materials exhibited weight gain and superior performance to a reference Zr-based alloy under hydrothermal environments. Although the corrosion behavior of the coating on SiC/SiC tubes has not been investigated, the information in Table 8 shows these coating materials are potentially useful for SiC cladding systems.

Table 8. Hydrothermal corrosion resistance of coated materials. The coated zirconium-based alloy was tested unless otherwise indicated

| Material          | Coating method            | Corrosion environment   | Corrosion test results  | Reference |
|-------------------|---------------------------|---|---|-----------|
| Bulk Cr           | Not applicable            | -360°C/18.9 MPa<br>- Static autoclave   | Weight gain of 3.2 mg/dm <sup>2</sup><br>after 15 days  | [68]      |
| Cr coating on Zr  | Physical vapor deposition | -360°C<br>-Simulated PWR primary water<br>-Autoclave  | Weight gain of ~5 mg/dm <sup>2</sup><br>after 60 days   | [69, 70]  |
| CrN coating on Zr | Physical vapor deposition | -300°C/pH <sub>25°C</sub> :10.5<br>-LiOH addition<br>-Static autoclave  | Better corrosion resistance<br>compared with Zr-4 after<br>30 days  | [73]      |
| CrN coating on Zr | Physical vapor deposition | -In-pile test<br>-PWR condition at 320°C<br>-150 days<br>-Fast neutron fluence: 1.8×10 <sup>24</sup> n/m <sup>2</sup> | Insignificant change in the<br>coating thickness by<br>irradiation<br>Local oxidation of the<br>substrate | [75]      |

### 3.3.2 Fuel-clad chemical interaction

The chemical compatibility of SiC cladding with fuels under normal operation and accident conditions is of great importance. The cladding inner surface comes in contact with the fuel, depending on the initial gap and the swelling behavior. Fission product transportation and interactions with SiC, SiC/SiC composites, the composite constituents, and internal interfaces also need to be understood for all gaseous and solid fission products. The fission products of primary interest include noble metals and tritium.

For an SiC/ $UO_{2+x}$  system, Braun et al. experimentally investigated the reactivity and concluded that (1) limited chemical reaction occurs up to 1241°C and (2) a liquid phase forms between 1577 and 1677°C in the open and closed SiC/ $UO_{2+x}$  system [76]. Silva et al. reported that the microstructure of high-purity SiC, such as the grain boundary structure, affected the chemical reaction between SiC and  $UO_2$  at 1500°C [77]. The reaction temperatures reported are much higher than the temperature of the cladding under normal operation.

Gerczak et al. discussed the potential reactions between SiC and various fission products, including fission gases, metallic precipitates, and oxide phases [78]. According to previous studies (typically a thin foil diffusion couple study), they concluded that SiC is susceptible to reaction with various fission product elements in the fuel system; however, the temperature of the SiC clad is not sufficient to promote significant interactions due to the reaction kinetics.

### 3.3.3 Steam oxidation

The oxidation resistance of CVD SiC, the expected first barrier against steam attack in CVI SiC/SiC tubes, is discussed in this section. Oxidation of SiC under a high-temperature steam environment is expressed by parabolic kinetics: parabolic oxidation forming silica on SiC and linear volatilization of the silica [3]. The parameters affecting the steam oxidation behavior include temperature, exposure time, steam flow rate, and steam pressure. Figure 10 shows the steam oxidation behavior of CVD SiC based on the experimental results (for SiC). An outstanding low recession rate for CVD SiC compared with Zircaloy-4 was reported. The results shown in Figure 10 are consistent with the results from different steam oxidation studies using high-purity CVD SiC [79], a CVD-coated CVI SiC/SiC composite [80], and sintered SiC (SE type Hexoloy) [81] under different steam oxidation conditions.

Monolithic SiC fabricated via liquid-phase sintering of SiC nanopowder and oxide additives, a similar material with a matrix of NITE SiC/SiC composite, also showed significant steam oxidation resistance compared with Zircaloy-4 at up to 1200°C [82], indicating NITE SiC/SiC cladding improves the safety of the cladding system in the case of an accident.

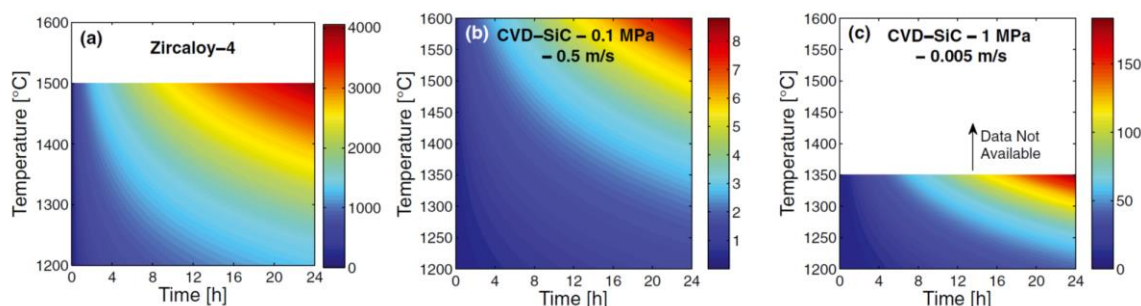


Figure 10. Thickness consumed (in  $\mu\text{m}$ ) during steam oxidation: (a) Zircaloy-4 and (b, c) CVD SiC. (Reprinted from Terrani 2014 [3])

## 4. IRRADIATED MATERIAL PROPERTIES

### 4.1 Physical and Thermal Properties

#### 4.1.1 Density

The density of SiC/SiC cladding changes as a result of irradiation-induced swelling. Accurate data for temperature- and dose-dependent swelling of SiC/SiC materials are essential for multi-physics modeling of the cladding. A swelling gradient across the clad thickness direction, resulting from the through-thickness temperature gradient, is a great concern because it builds significant stress within the cladding [83]. Although swelling of SiC/SiC plates has been evaluated for various irradiation conditions [6], and those data are applicable to the tube specimens, we report recent swelling results with improved measurement accuracy.

The dimensions of the specimens were measured using a precision micrometer. The micrometer used was equipped with a high-precision linear variable differential transformer, and its calibration was maintained to an accuracy of  $\pm 0.1$  micron at all times through a calibration procedure using standard gauge blocks incorporated in the specimen measurement protocol. All three dimensions of the rectangular coupon specimens were measured using the micrometer. The length of all specimens was 25 mm (Figure 11).

The neutron irradiation experiments were conducted in the High Flux Isotope Reactor (HFIR) at Oak Ridge National Laboratory (ORNL). The measurement results in Figure 12 show that swelling behavior is almost identical among the CVD SiC and CVI SiC/SiC composites in the length direction (an in-plane direction). The swelling of neutron-irradiated SiC/SiC tubes [8, 84] appeared to follow the trend. Details for the materials investigated are shown in Table 9.

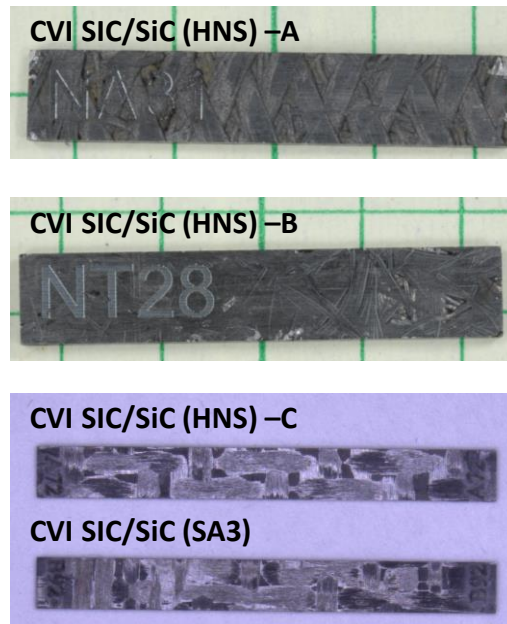


Figure 11. Representative image of test specimens used for irradiation experiment. Length of all specimens was 25 mm. Details for each material are shown in Table 9.

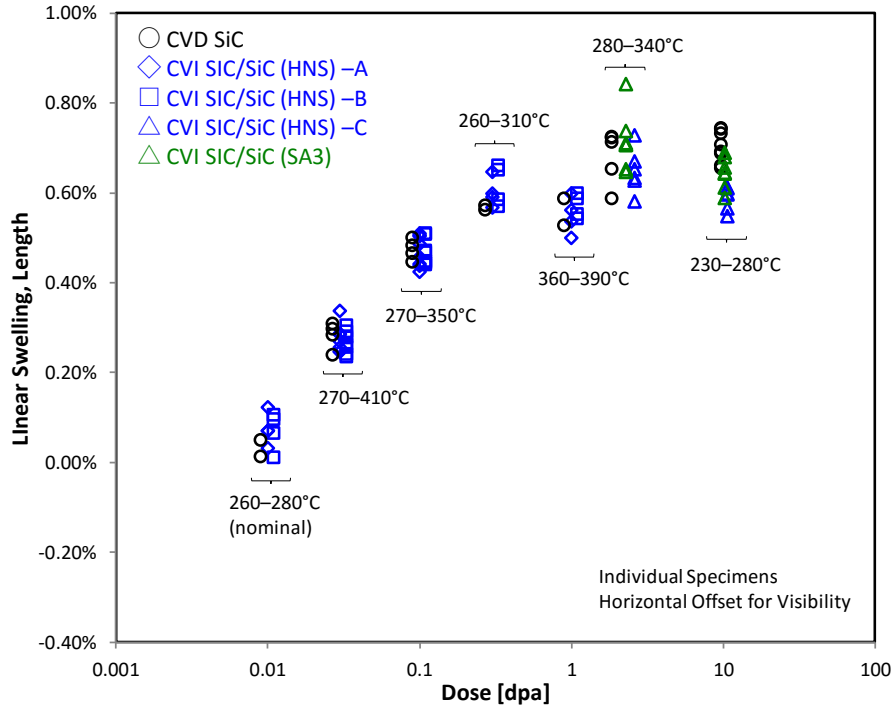


Figure 12. Linear swelling of CVD SiC and SiC/SiC plates. Details for the materials investigated are shown in Table 9.

Table 9: Information for CVD SiC and SiC/SiC composite materials used for swelling measurements

| Material ID          | Material description   | Specimen dimensions                                   | Reference                |
|----------------------|--|---|--------------------------|
| CVD SiC              | Monolithic   | 50×2.5×2.5 mm or<br>50×5.0×0.2 mm or<br>25×2.8×0.4 mm | Unpublished data<br>[85] |
| CVI SiC/SiC (HNS) -A | Machined from channel box. The length direction parallel to axial length direction of the channel box. | 25×4.5×1.3 mm   | Unpublished data         |
| CVI SiC/SiC (HNS) -B | Machined from channel box. The length direction parallel to axial width direction of the channel box.  | 25×4.5×1.3 mm   | Unpublished data         |
| CVI SiC/SiC (HNS) -C | Fiber reinforcements parallel to the specimen length and width directions                              | 25×2.8×1.0 mm   | [85]                     |
| CVI SiC/SiC (SA3)    | Fiber reinforcements parallel to the specimen length and width directions                              | 25×2.8×1.0 mm   | [85]                     |

A new finding of this work is that the CVI SiC/SiC plates showed swelling anisotropy, as shown in Figure 13. The order of the magnitude of the swelling was length > width > thickness. This indicates that the swelling of an SiC/SiC cladding along the thickness direction may be less than in the length direction. This swelling anisotropy will affect the multi-physics modeling of the stress states of SiC/SiC cladding. This work is under preparation for publication in a journal.

This research also produced a precise description of the swelling of CVD and CVI SiC/SiC composites, as shown in Figure 14. This was achieved by measuring both the swelling and the actual irradiation temperature with the same specimens so that the experimental uncertainty was minimized.



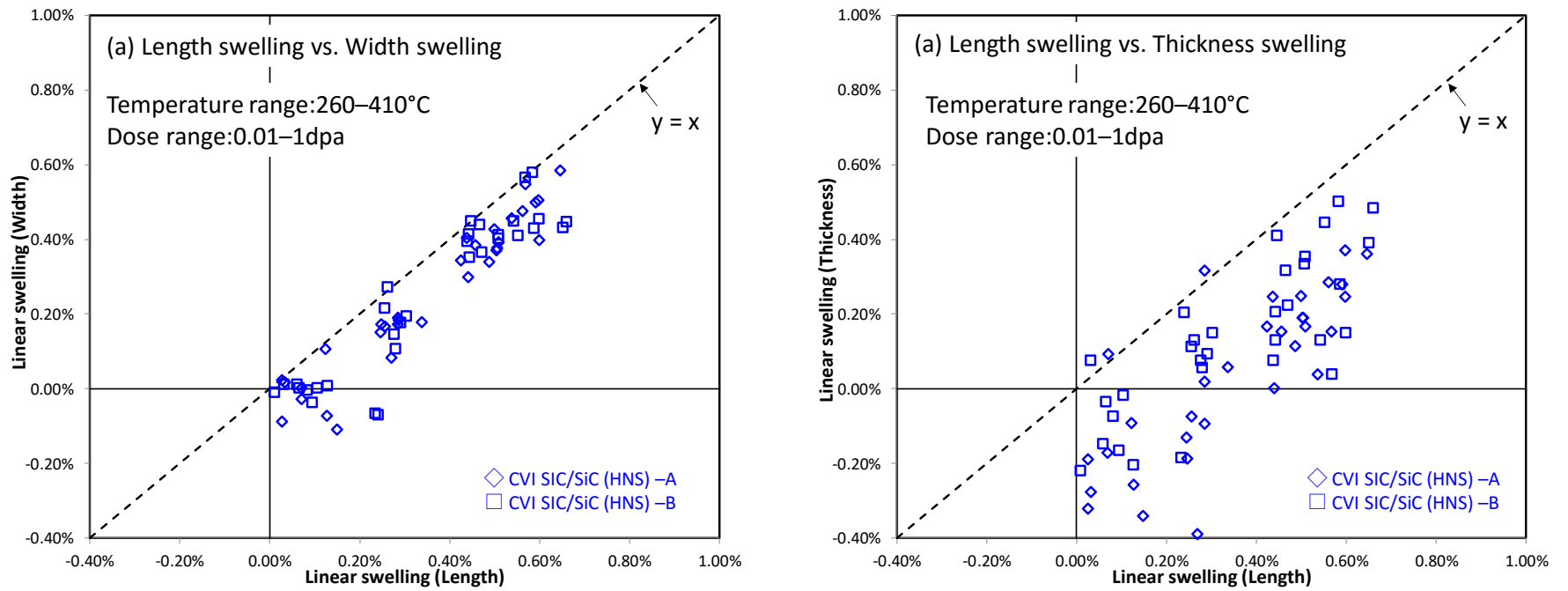


Figure 13. Anisotropic swelling of CVI SiC/SiC plates. The relationship between specimen direction and fiber architecture is shown in Table 9.

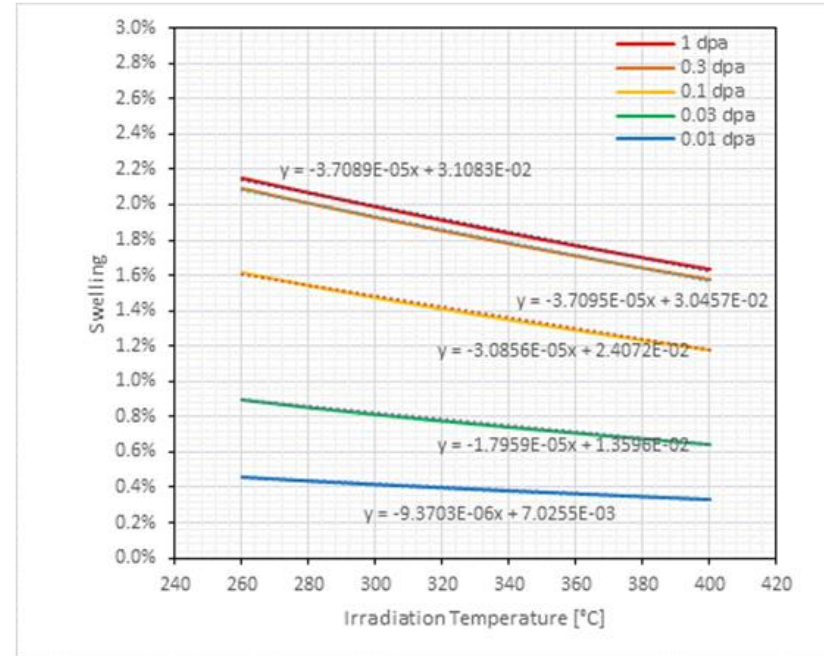
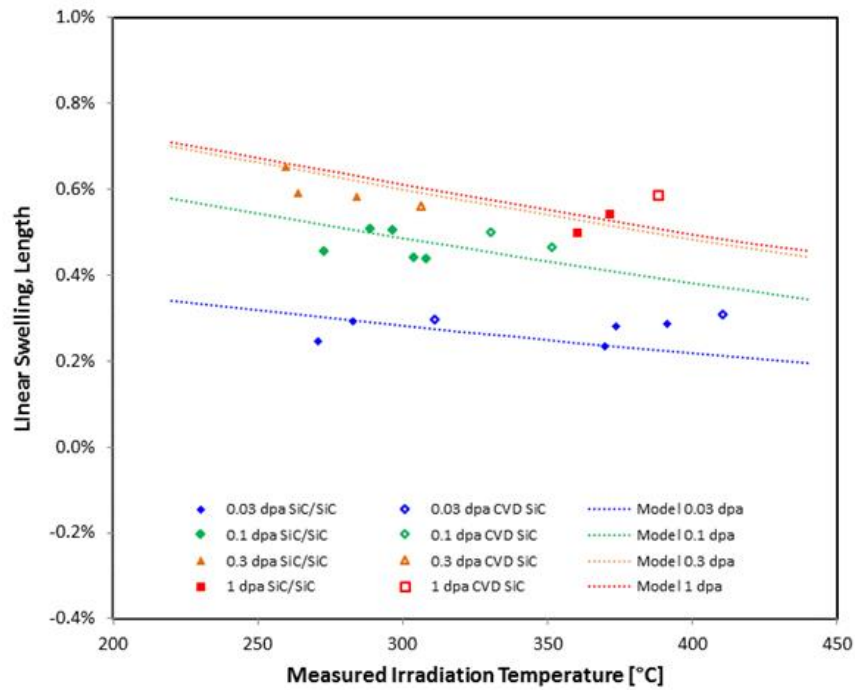


Figure 14. Temperature and dose dependence of swelling of CVD SiC and CVI SiC/SiC composites.

### 4.1.2 Fiber volume fraction and porosity

Although differential swelling behavior was found, as shown in the previous section, the effect of irradiation on the fiber volume fraction was negligible because of the small swelling value (up to ~2% in volume). It is also expected that irradiation will not change the porosity.

### 4.1.3 Thermal expansion

Since very limited data are available for the CTEs of SiC/SiC composites irradiated under LWR-relevant temperature and dose conditions, this report presents instantaneous CTEs for HNS fiber-reinforced CVI SiC/SiC composite plates neutron-irradiated at 360 or 370°C to 1dpa under an inert atmosphere in the HFIR, as shown in Figure 15. Dilatometry of the irradiated ~24 mm long specimens was conducted using a NETZSCH DIL 402CD horizontal dual pushrod dilatometer with a heating rate of 1°C/min and a cooling rate of 2.5°C/min. It was found that the instantaneous CTE of the neutron-irradiated SiC/SiC was described by the CTE of nonirradiated SiC/SiC composites (Eq. (1)) up to the irradiation temperature, showing that the effect of irradiation on the CTE was insignificant. This is consistent with a previous study of the CTE of SiC/SiC composites irradiated at higher temperatures [6]. Note that, above the irradiation temperature, the CTE was apparently small because of recovery of swelling by defect recovery.

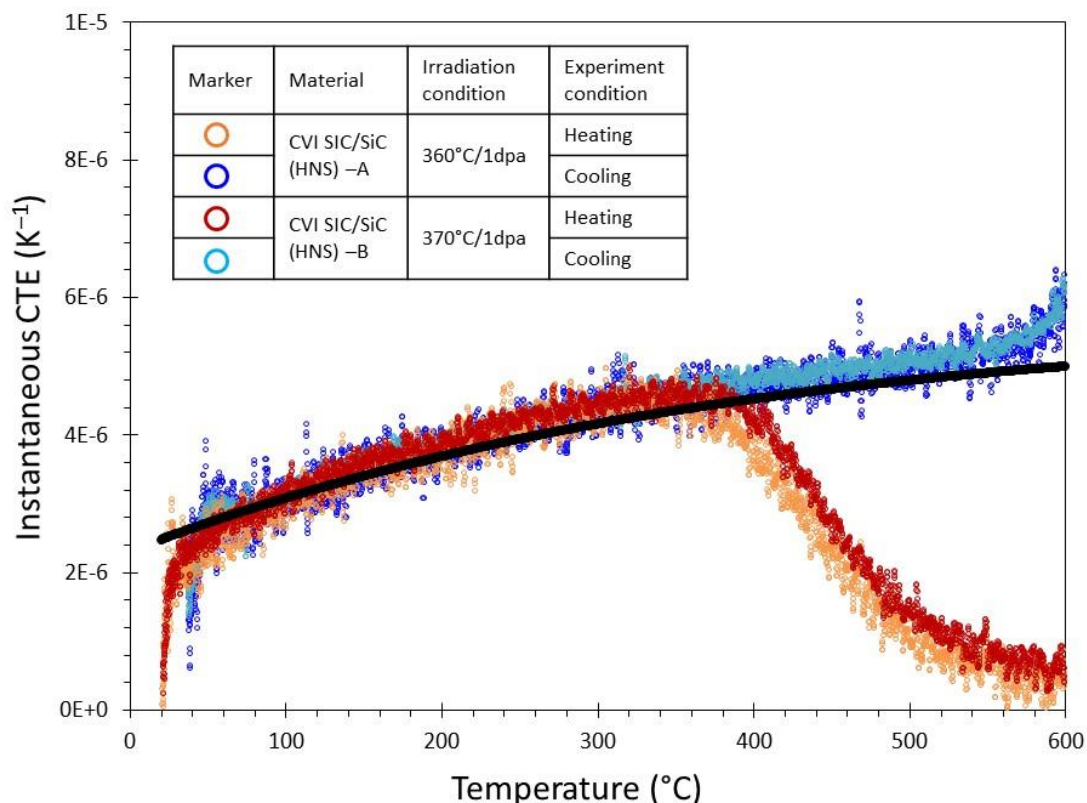


Figure 15. Instantaneous CTE of neutron-irradiated CVI SiC/SiC composite plates. The black line is the trend of nonirradiated materials, which is described in Eq. (1). The material information can be found in Table 9.

#### 4.1.4 Thermal diffusivity and thermal conductivity

Since there are no thermal diffusivity data for SiC tubes obtained by a standard method, no reliable thermal properties data are available for neutron-irradiated SiC tubes. In such a situation, it would be reasonable to use the thermal properties obtained from the plate specimens for modeling purposes. The effect of irradiation on the thermal conductivity of ceramics is described by the thermal resistivity, the inverse of thermal conductivity,  $K$  [86]:

$$\frac{1}{K_{rd}} = \frac{1}{K_{irr}} + \frac{1}{K_{non-irr}} \quad (6)$$

where  $1/K_{irr}$  and  $1/K_{non-irr}$  indicate irradiated and nonirradiated thermal resistivity, respectively, and  $1/K_{rd}$  is the radiation defect thermal resistivity that represents collective contributions from various radiation-produced defects to the volume thermal resistivity.

Figure 16 shows the room-temperature defect thermal resistivity of SiC/SiC plate specimens and monolithic CVD SiC [6], together with the defect thermal resistivity of neutron-irradiated SiC tubes evaluated by the laser flash method with a curved specimen [8]. It is clear that the defect thermal resistivity of the plate specimens is material-dependent. The results from the tube specimens reported in [8] appeared to be consistent with the results from the plate specimens. Note that the triplex tube specimen [8] was expected to be greatly affected by the monolithic layer because of its volume fraction. The dose dependence of irradiation thermal defect resistivity can be obtained from a linear relationship between the thermal defect resistivity and the swelling [87]. Because very limited thermal properties data for the SiC/SiC cladding are available, future work on this topic requires (1) the development of a standard test method for the thermal properties evaluation of ceramic tubes and (2) an evaluation of the thermal properties of SiC-based tubes irradiated under LWR-relevant temperatures and doses.

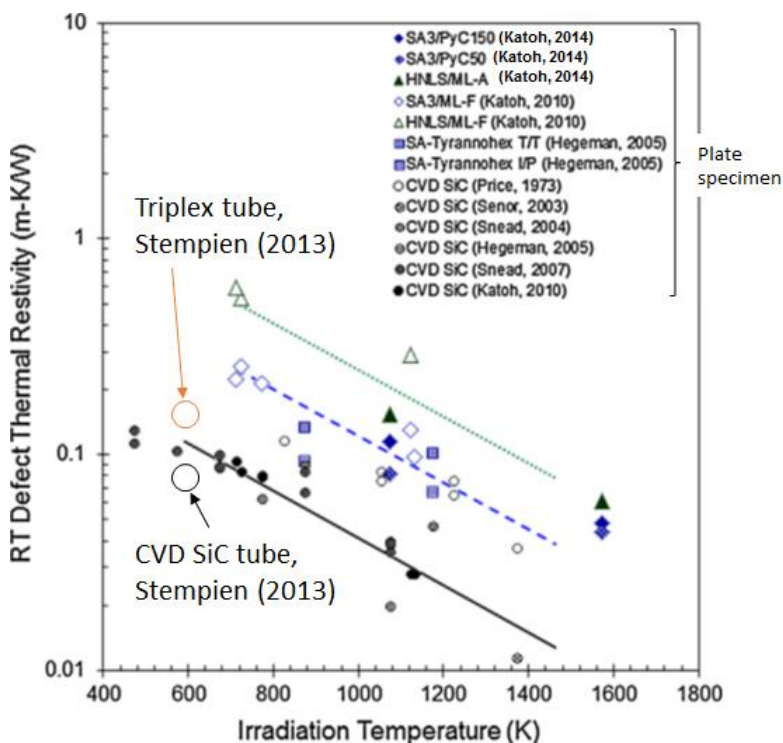


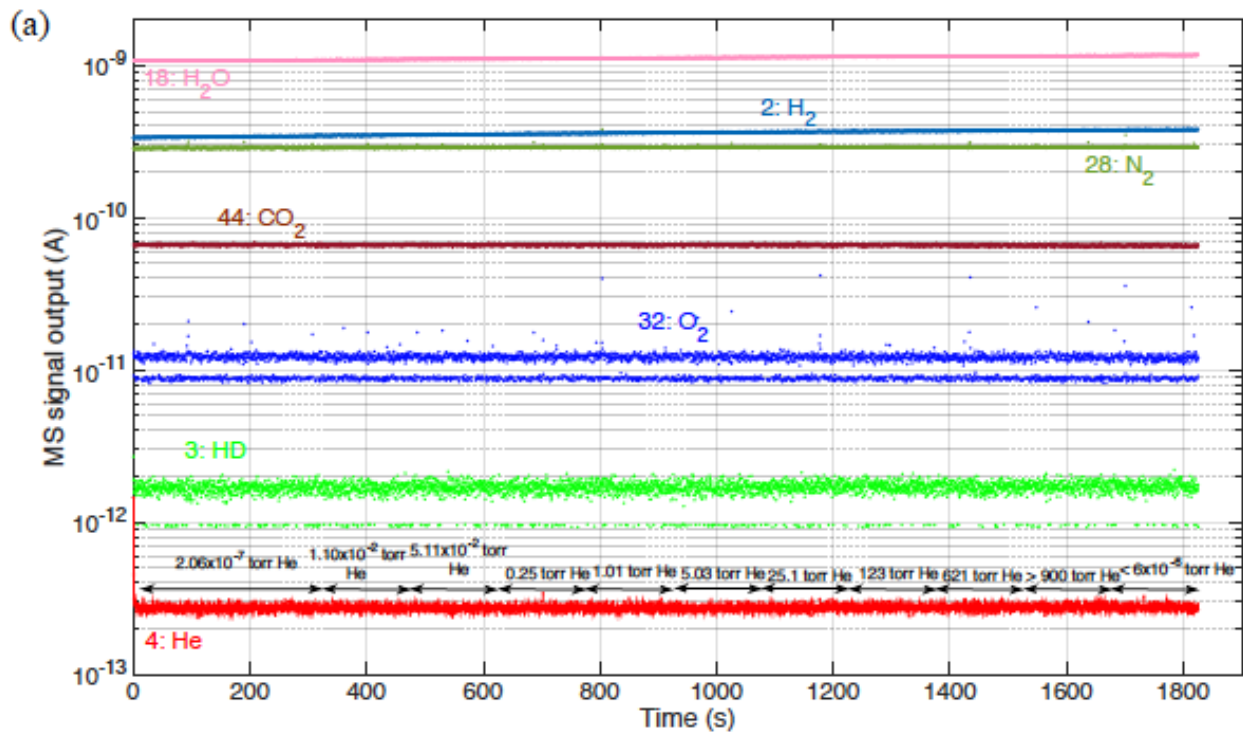
Figure 16. Room-temperature radiation defect thermal resistivity of neutron-irradiated SiC/SiC composites and monolithic CVD SiC plotted against irradiation temperature [6, 8]. The neutron dose ranged from 0.8 to 11.7 dpa for composites.

### 4.1.5 Specific heat

The effect of neutron irradiation on the specific heat of the SiC/SiC tube was negligible because of the limited change in the density following irradiation [61, 88].

### 4.1.6 Permeability

At this point, there is no report on the permeability of SiC/SiC composites in tubular configurations subject to neutron irradiation. This study reports the gas permeability of neutron-irradiated CVD SiC tubes following neutron irradiation at  $\sim 300^\circ\text{C}$  to  $\sim 2$  dpa with a high heat flux. Detailed material information and irradiation conditions can be found elsewhere [84]. Following the same procedure used in testing of nonirradiated samples shown in Hu et al. (2017) [64], the helium and deuterium permeation flux through a neutron-irradiated CVD SiC tube was measured. The results, shown in Figure 17, indicate that the tested CVD SiC tubular sample following neutron irradiation is still hermetic, as manifested by the extremely low helium and deuterium permeation fluxes at various gas pressures. This finding implies that CVD SiC-coated SiC/SiC cladding is hermetic following neutron irradiation.



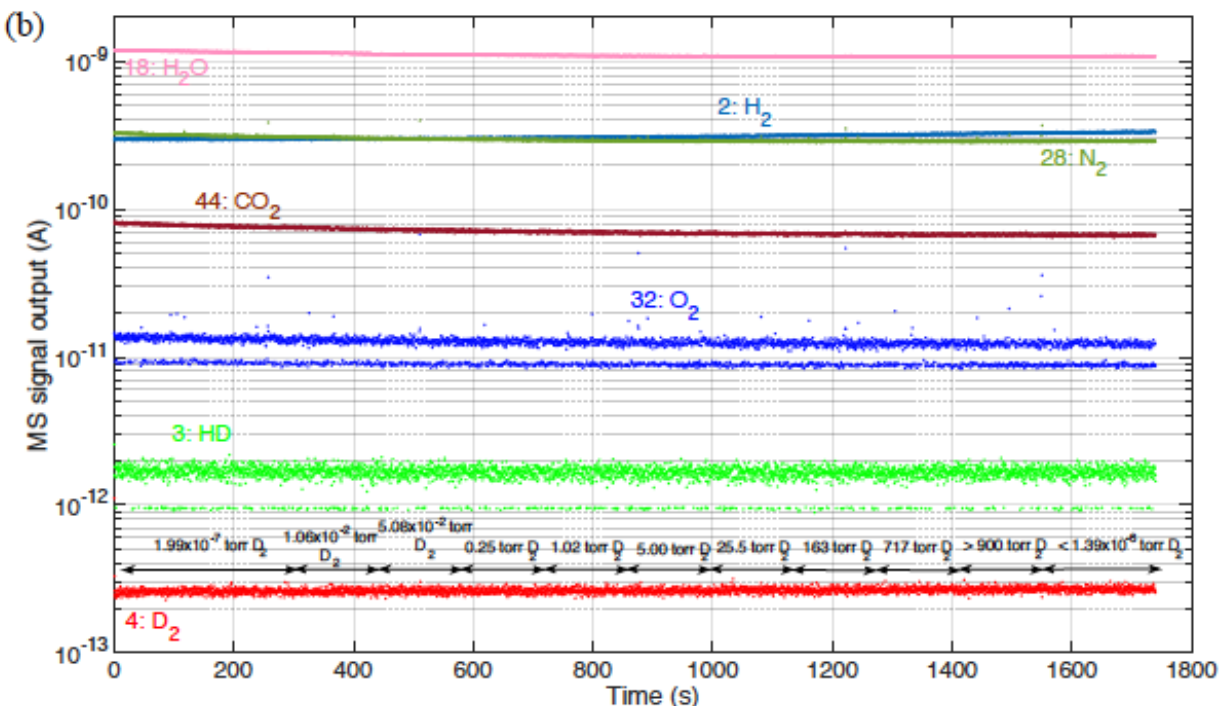


Figure 17. (a) Helium and (b) deuterium permeation fluxes through neutron-irradiated CVD SiC as a function of applied gas pressure [64].

## 4.2 Mechanical Properties

Since mechanical properties data for irradiated SiC/SiC tubes are highly limited, the mechanical properties of irradiated SiC/SiC composite plates are presented. Table 10 lists the reported mechanical properties of SiC/SiC plates neutron-irradiated under LWR-relevant dose and temperature conditions. Although the available data are limited, Table 10 shows that no notable irradiation-induced degradation of mechanical properties (e.g., Young's modulus, PLS, ultimate strength) was found for CVI SiC/SiC composites with SA3 or HNS coated multi-layer or single-layer PyC. Recent work by Koyanagi and Katoh (2017) [85] shows no notable effect of irradiation at  $\sim 300^\circ\text{C}$  up to 11.8 dpa on the flexural behavior of CVI SiC/SiC composites with monolayer PyC-coated HNS or SA3 fibers (Figure 18). Therefore, it is reasonable to assume that the effects of irradiation on the mechanical properties are negligible for modeling during normal operation. However, mechanical degradation may be taken into account in the model at high doses because both HNS fiber and multi-layer PyC/SiC interphase were degraded at a high dose of  $\sim 40$  dpa at 300 and  $500^\circ\text{C}$  [88]. Currently, no data are available for the mechanical properties of NITE SiC/SiC composites, although the tensile properties were retained following neutron irradiation at  $600^\circ\text{C}$  to 0.52 dpa, at  $830^\circ\text{C}$  to 5.9 dpa, and at  $1270^\circ\text{C}$  to 5.8 dpa [89].

Table 10. Mechanical properties of CVI SiC/SiC composites nonirradiated and irradiated under LWR-relevant temperature and dose conditions.  
All the irradiation experiments were carried out under an inert gas atmosphere in the HFIR

| Material<br>(Interphase type)  | Irradiation conditions         | Test method        | Young's modulus<br>(GPa) | Proportional limit<br>stress<br>(MPa) | Ultimate strength<br>(MPa)   | Reference |
|--|--------------------------------|--------------------|--------------------------|---------------------------------------|------------------------------|-----------|
| HNS CVI SiC/SiC plate<br>(PyC <sub>20 nm</sub> /SiC <sub>100 nm</sub> multi-<br>layer) | Nonirradiated 1                | Cyclic tensile     | 232 (25)                 | 97 (24)                               | 284 (19)                     | [90]      |
|  | Nonirradiated 2                |                    | 226 (27)                 | 126 (12)                              | 224(13)                      |           |
|  | 570°C/2.2 dpa                  |                    | 197 (19)                 | 116 (12)                              | 171 (38)                     |           |
| HNS CVI SiC/SiC plate<br>(PyC <sub>20 nm</sub> /SiC <sub>100 nm</sub> multi-<br>layer) | Nonirradiated<br>300°C/3.4 dpa | 4 point flexural   | Not available            | 375.0 (50.9)<br>332.4 (4.5)           | 469.9 (70.1)<br>420.4 (29.8) | [91]      |
| HNS CVI SiC/SiC plate<br>(PyC 50–160 nm)   | Nonirradiated                  | Dynamic<br>modulus | 255 (6)                  | 216 (8)                               | 412 (35)                     | [85]      |
|  | 280–340°C/2.0 dpa              |                    | 236 (24)                 | 260 (28)                              | 509 (49)                     |           |
|  | 230–280°C/11.8 dpa             | 4 point flexural   | 210 (13)                 | 226 (45)                              | 486 (72)                     |           |
| SA3 CVI SiC/SiC plate<br>(PyC 200–350 nm)  | Nonirradiated                  | Dynamic<br>modulus | 241 (11)                 | 331 (91)                              | 493 (59)                     | [85]      |
|  | 280–340°C/2.0 dpa              |                    | 241 (22)                 | 300 (40)                              | 513 (87)                     |           |
|  | 230–280°C/11.8 dpa             | 4 point flexural   | 220 (7)                  | 344 (85)                              | 482 (74)                     |           |

Note: values in brackets are standard deviations.

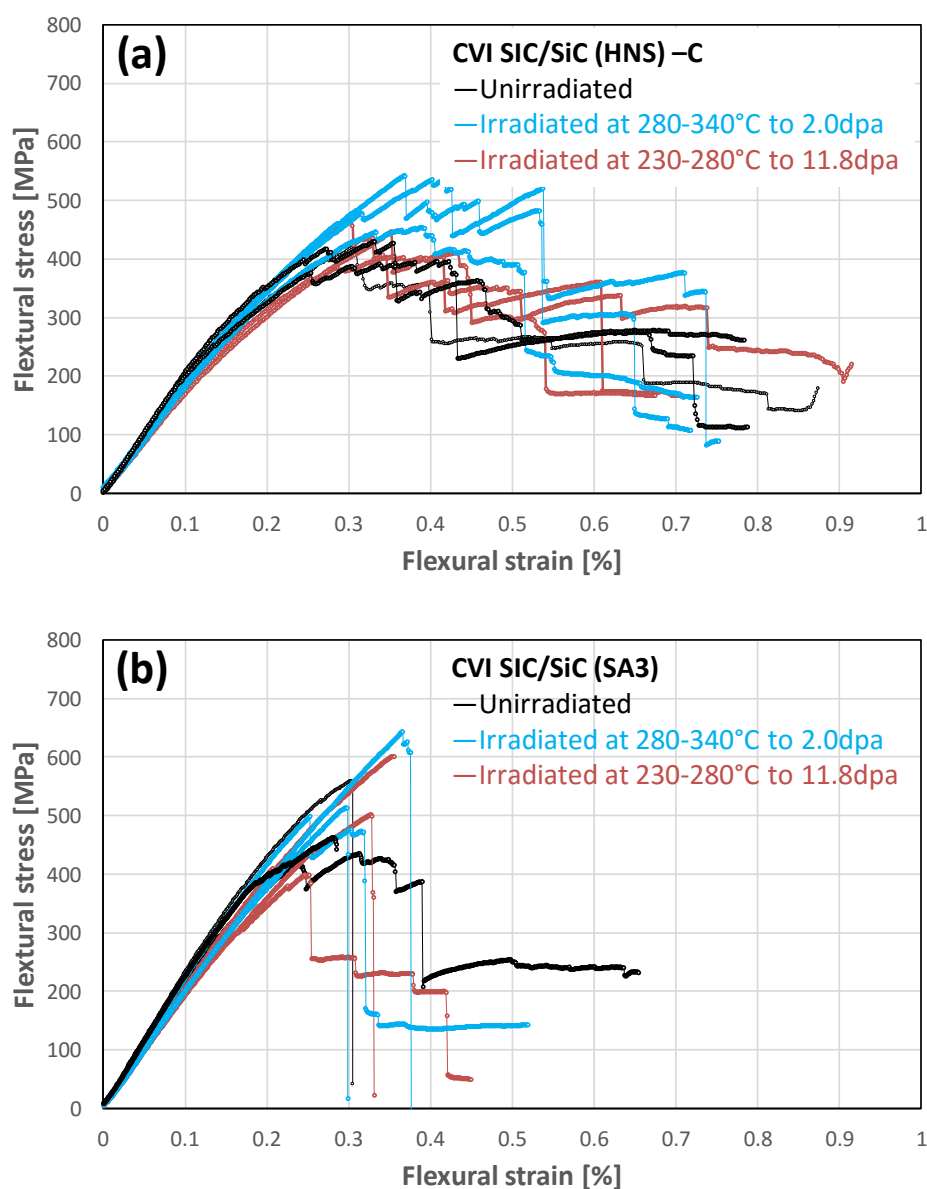


Figure 18. Flexural stress strain curves for (a) CVI SiC/SiC (HNS)-C and (b) CVI SiC/SiC (SA3) for nonirradiated and irradiated conditions [85].

The specimen information can be found in Table 9. Effects of irradiation on the strength of selected SiC plate to plate joints are summarized in Table 11 [30, 92]. The irradiation was conducted at 280–310°C to 8.7 dpa, which is relevant to LWR applications. The substrate was monolithic CVD SiC for all the cases. Torsional shear testing using a miniature hourglass specimen was conducted. Note that the obtained strength is apparent because of nonuniform stress distribution within the specimen during the testing. Details of the interpretation of the torsion strength can be found elsewhere [93, 94]. As shown in Table 11, all the joints exhibited relatively high values (>80 MPa on average) of apparent shear strength following neutron irradiation. However, irradiation-induced cracking within the bonding layer typically was found in the non-SiC bonding layers. Although the strength of the cracked joint was relatively high, the cracking may result in the loss of the gas leak tightness of the joints. Future work is needed to



demonstrate robust and hermetic SiC joints with an end-plug configuration, since the bonding quality may be different between plate-to-plate joints and end-plug joints.

Table 11. Apparent shear strength of various SiC joints with and without irradiation. The substrate was monolithic CVD SiC for all cases. Torsion tests using a miniature hourglass specimen were conducted to obtain the data.

| Joining method<br>(joint phases)  | Conditions  | Apparent shear strength [MPa] | Note  | Reference |
|---|---|-------------------------------|---|-----------|
| Titanium foil diffusion<br>(Ti <sub>3</sub> SiC <sub>2</sub> , TiSi <sub>2</sub> )        | Nonirradiated<br>Irradiated at 280–<br>310°C to 8.7 dpa | 133 (22)<br>86 (66)           | Irradiation-induced<br>cracking                         | [92]      |
| Molybdenum foil diffusion<br>(Mo <sub>&lt;5</sub> Si <sub>3</sub> C<1, Mo <sub>2</sub> C) | Nonirradiated<br>Irradiated at 280–<br>310°C to 8.7 dpa | 146 (14)<br>84 (6)            |   |           |
| SiC nanopowder slurry<br>sintering<br>(SiC, Y-Al-Zr oxides)                               | Nonirradiated<br>Irradiated at 280–<br>310°C to 8.7 dpa | 320 (31)<br>226 (156)         | No obvious<br>microstructural change<br>by irradiation  |           |
| SiC nano-powder green<br>sheet sintering<br>(SiC, Y-Al-Zr oxides)                         | Nonirradiated<br>Irradiated at 280–<br>310°C to 8.7 dpa | 116 (24)<br>109 (54)          |   |           |
| Ti-Si-C reaction sintering<br>(Ti <sub>3</sub> SiC <sub>2</sub> , SiC, minor TiC)         | Nonirradiated<br>Irradiated at 280–<br>310°C to 8.7 dpa | 147 (12)<br>123 (13)          | Irradiation-induced<br>cracking                         |           |
| Hybrid polymer/CVI SiC<br>(SiC)   | Nonirradiated<br>Irradiated at 280–<br>310°C to 8.7 dpa | 93 (12)<br>93 (17)            | No obvious<br>microstructural change<br>by irradiation  |           |
| Brazing<br>(Al-Si-C-O)  | Nonirradiated<br>Irradiated at 280–<br>310°C to 8.7 dpa | 138 (20)<br>190 (10)          | No obvious<br>microstructural change<br>by irradiation* |           |

\*Unpublished result

Note: values in brackets are standard deviation

### 4.3 In-Pile Hydrothermal Corrosion

Neutron irradiation is an important factor affecting hydrothermal corrosion; the radiolysis of light water increases the concentrations of oxidizing radiolytic species [95], and irradiation-induced defects may change the reactivity of the material. Previous in-pile tests at the Massachusetts Institute of Technology reactor—with open-ended CVI SiC/SiC composite tube samples in a simulated PWR coolant with 10.3 MPa pressure at 300°C—showed a significant increase in weight loss compared with corrosion without irradiation [8]. An autoclave test with ion-irradiated CVD SiC samples [96] also indicated accelerated corrosion with irradiation. Although the data are limited, irradiation-assisted corrosion of the SiC likely occurred. Stempien et al. (2013) report in-pile corrosion behaviors in SiC plate joints bonded using TiC/SiC tape, calcium aluminate glass, or titanium foil [8]. All types of these joints were completely or partially debonded during the simulated PWR reactor coolant exposure for 44 days at an irradiation dose of up to 0.16 dpa for SiC. Although the presence of irradiation-enhanced corrosion is not clearly addressed in Stempien et al. [8], the development of a corrosion-tolerant joint is a critical issue. The in-pile corrosion behavior of coatings also is rarely reported.

The current state of knowledge in the area of corrosion of SiC fuel cladding in LWR coolant environments is very shallow, presenting what is perhaps the biggest current knowledge gap for this technology. Systematic tests with well-defined samples, under well-known conditions, aiming to quantify the kinetics and identify the mechanism for corrosion, are necessary.

## 5. FUTURE DIRECTION

This report summarizes various physical and mechanical properties of SiC composites for LWR cladding applications. To provide relatively complete information for SiC/SiC composites (the ultimate purpose of this handbook), other properties need to be added in future publications, including the thermal conductivity of the tubes, in-pile hydrothermal corrosion, and fuel-chemical and mechanical interactions of irradiated SiC tubes. Statistical failure assessment of SiC tubes is also needed to assess the failure probability of the fuel system. These properties are being evaluated with support from the Advanced Fuels Campaign of the US Department of Energy (DOE) Nuclear Technology R&D program.

## 6. ACKNOWLEDGMENTS

The authors would like to thank Xunxiang Hu for critical review of the report. The research is sponsored by the Advanced Fuels Campaign of the Nuclear Technology R&D program, Office of Nuclear Energy, DOE, under contract DE-AC05-00OR22725 with UT-Battelle, LLC. A portion of this research used resources at the HFIR, a DOE Office of Science User Facility operated by ORNL. This work also used resources at the Low Activation Materials Development and Analysis Laboratory at ORNL.

## 7. REFERENCES

1. Parisi, C., et al., *Simulation & analysis of the severe accident of the Unit 1 of Fukushima Daiichi NPP*. Energia, Ambiente e Innovazione, 2012. **2**: p. 56-61.
2. Zinkle, S.J., et al., *Accident tolerant fuels for LWRs: A perspective*. Journal of Nuclear Materials, 2014. **448**(1): p. 374-379.
3. Terrani, K.A., et al., *Silicon carbide oxidation in steam up to 2 MPa*. Journal of the American Ceramic Society, 2014. **97**(8): p. 2331-2352.
4. Katoh, Y., et al., *Radiation effects in SiC for nuclear structural applications*. Current Opinion in Solid State and Materials Science, 2012. **16**(3): p. 143-152.
5. Katoh, Y. and K.A. Terrani, *Systematic Technology Evaluation Program for SiC/SiC Composite-based Accident-Tolerant LWR Fuel Cladding and Core Structures: Revision 2015*. 2015, Oak Ridge National Laboratory (ORNL).
6. Katoh, Y., et al., *Continuous SiC fiber, CVI SiC matrix composites for nuclear applications: Properties and irradiation effects*. Journal of Nuclear Materials, 2014. **448**(1): p. 448-476.
7. Deck, C., et al., *Characterization of SiC-SiC composites for accident tolerant fuel cladding*. Journal of Nuclear Materials, 2015. **466**: p. 667-681.
8. Stempien, J.D., et al., *Characteristics of composite silicon carbide fuel cladding after irradiation under simulated PWR conditions*. Nuclear Technology, 2013. **183**(1): p. 13-29.
9. Kim, D., et al., *Fabrication and measurement of hoop strength of SiC triplex tube for nuclear fuel cladding applications*. Journal of Nuclear Materials, 2015. **458**: p. 29-36.
10. Jung, Y.I., S.-H. Kim, and J.-Y. Park, *Manufacturing process for the metal-ceramic hybrid fuel cladding tube*. Trans. Korean Nucl. Soc, 2012: p. 25-26.

11. Ang, C.K., et al., *Examination of Hybrid Metal Coatings for Mitigation of Fission Product Release and Corrosion Protection of LWR SiC/SiC*. 2016, Oak Ridge National Laboratory (ORNL), Oak Ridge, TN (United States).
12. Sauder, C., *Ceramic matrix composites: nuclear applications*. Ceramic Matrix Composites: Materials, Modeling and Technology, 2014: p. 609-646.
13. Snead, L., D. Steiner, and S. Zinkle, *Measurement of the effect of radiation damage to ceramic composite interfacial strength*. Journal of nuclear materials, 1992. **191**: p. 566-570.
14. Takeda, M., et al., *Effect of hydrogen atmosphere on pyrolysis of cured polycarbosilane fibers*. Journal of the American Ceramic Society, 2000. **83**(5): p. 1063-1069.
15. Ichikawa, H., *Development of high performance SiC fibers derived from polycarbosilane using electron beam irradiation curing-a review*. Journal of the Ceramic Society of Japan, 2006. **114**(1330): p. 455-460.
16. Ishikawa, T., et al., *High-strength alkali-resistant sintered SiC fibre stable to 2,200 C*. Nature, 1998. **391**(6669): p. 773-775.
17. Lipowitz, J., et al. *Structure and Properties of Sylramic™ Silicon Carbide Fiber—A Polycrystalline, Stoichiometric  $\beta$  - Sic Composition*. in *Proceedings of the 21st Annual Conference on Composites, Advanced Ceramics, Materials, and Structures: A: Ceramic Engineering and Science Proceedings, Volume 18, Issue 3*. 1997. Wiley Online Library.
18. Bansal, N.P., *Handbook of ceramic composites*. Vol. 200. 2006: Springer Science & Business Media.
19. Katoh, Y., T. Nozawa, and L.L. Snead, *Mechanical Properties of Thin Pyrolytic Carbon Interphase SiC–Matrix Composites Reinforced with Near - Stoichiometric SiC Fibers*. Journal of the American Ceramic Society, 2005. **88**(11): p. 3088-3095.
20. Hinoki, T. and A. Kohyama, *Current status of SiC/SiC composites for nuclear applications*. Annales de Chimie. Science des Matériaux (Paris), 2005. **30**(6): p. 659-671.
21. Hinoki, T., et al., *Silicon carbide and silicon carbide composites for fusion reactor application*. Materials Transactions, 2013. **54**(4): p. 472-476.
22. Deck, C., et al., *Fabrication of SiC–SiC composites for fuel cladding in advanced reactor designs*. Progress in Nuclear Energy, 2012. **57**: p. 38-45.
23. Uchihashi, M., et al. *ICONE23-1387 DEVELOPMENT OF SIC/SIC COMPOSITE FOR NUCLEAR REACTOR CORE WITH ENHANCED SAFETY*. in *The Proceedings of the International Conference on Nuclear Engineering (ICONE) 2015.23*. 2015. The Japan Society of Mechanical Engineers.
24. Katoh, Y., S. Dong, and A. Kohyama, *Thermo-mechanical properties and microstructure of silicon carbide composites fabricated by nano-infiltrated transient eutectoid process*. Fusion Engineering and Design, 2002. **61**: p. 723-731.
25. Kohyama, A., *“Inspire” Project for R&D of Sic/Sic Fuel Cladding by Nite Method*. Ceramics for Environmental and Energy Applications II: Ceramic Transactions, Volume 246, 2014: p. 99-107.
26. Parish, C.M., et al., *Microstructure and hydrothermal corrosion behavior of NITE-SiC with various sintering additives in LWR coolant environments*. Journal of the European Ceramic Society, 2017. **37**: p. 1261-1279.
27. Duan, Z., et al., *Current status of materials development of nuclear fuel cladding tubes for light water reactors*. Nuclear Engineering and Design, 2017. **316**: p. 131-150.
28. Spitsberg, I. and J. Steibel, *Thermal and environmental barrier coatings for SiC/SiC CMCs in aircraft engine applications*. International Journal of Applied Ceramic Technology, 2004. **1**(4): p. 291-301.
29. Katoh, Y., et al., *Current status and recent research achievements in SiC/SiC composites*. Journal of Nuclear Materials, 2014. **455**(1): p. 387-397.
30. Fellowsa, J., et al., *Low Temperature Air Braze Process for Joining Silicon Carbide Components used in Heat Exchangers, Fusion and Fission Reactors, and Other Energy Production and*

- Chemical Synthesis Systems*. Ceramic Materials for Energy Applications VI: Ceramic Engineering and Science Proceedings Volume 37, 2017(6): p. 3.
31. Khalifa, H., et al., *Fabrication and characterization of joined silicon carbide cylindrical components for nuclear applications*. Journal of Nuclear Materials, 2015. **457**: p. 227-240.
  32. Sha, J., et al., *Effect of heat treatment on the tensile strength and creep resistance of advanced SiC fibers*. Journal of nuclear materials, 2004. **329**: p. 592-596.
  33. DeLeeuw, D., *Effects of Joining Pressure and Deformation on the Strength and Microstructure of Diffusion - Bonded Silicon Carbide*. Journal of the American Ceramic Society, 1992. **75**(3): p. 725-727.
  34. Moore, T.J., *Feasibility study of the welding of SiC*. Journal of the American Ceramic Society, 1985. **68**(6).
  35. Cockeram, B., *The diffusion bonding of silicon carbide and boron carbide using refractory metals*. 1999, Bettis Atomic Power Lab., West Mifflin, PA (US).
  36. Jung, Y.-I., et al., *Effect of Ti and Si Interlayer Materials on the Joining of SiC Ceramics*. Nuclear Engineering and Technology, 2016.
  37. McDermid, J.R. and R.A. Drew, *Thermodynamic brazing alloy design for joining silicon carbide*. Journal of the American Ceramic Society, 1991. **74**(8): p. 1855-1860.
  38. Liu, Y., Z. Huang, and X. Liu, *Joining of sintered silicon carbide using ternary Ag-Cu-Ti active brazing alloy*. Ceramics International, 2009. **35**(8): p. 3479-3484.
  39. Lippmann, W., et al., *Laser joining of silicon carbide—a new technology for ultra-high temperature resistant joints*. Nuclear Engineering and Design, 2004. **231**(2): p. 151-161.
  40. Ferraris, M., et al., *Joining of SiC-based materials for nuclear energy applications*. Journal of Nuclear Materials, 2011. **417**(1): p. 379-382.
  41. Colombo, P., et al., *Joining of reaction-bonded silicon carbide using a preceramic polymer*. Journal of Materials Science, 1998. **33**(9): p. 2405-2412.
  42. Lewinsohn, C.A., et al., *Silicon carbide-based materials for joining silicon carbide composites for fusion energy applications*. Journal of Nuclear Materials, 2002. **307**: p. 1232-1236.
  43. Singh, M., *Microstructure and mechanical properties of reaction-formed joints in reaction-bonded silicon carbide ceramics*. Journal of materials science, 1998. **33**(24): p. 5781-5787.
  44. Henager, C.H. and R.J. Kurtz, *Low-activation joining of SiC/SiC composites for fusion applications*. Journal of Nuclear Materials, 2011. **417**(1): p. 375-378.
  45. Koyanagi, T., et al., *Hydrothermal corrosion of silicon carbide joints without radiation*. Journal of Nuclear Materials, 2016.
  46. Hinoki, T., et al., *Development of joining and coating technique for SiC and SiC/SiC Composites utilizing NITE processing*. Mechanical Properties and Performance of Engineering Ceramics and Composites: Ceramic Engineering and Science Proceedings, Volume 26, Number 2, 2005: p. 399-405.
  47. Iseki, T., K. Arakawa, and H. Suzuki, *Joining of dense silicon carbide by hot-pressing*. Journal of Materials Science, 1980. **15**(4): p. 1049-1050.
  48. Tian, W., et al., *Effect of composition and joining parameters on microstructure and mechanical properties of silicon carbide joints*. Journal of the Ceramic Society of Japan, 2010. **118**(1381): p. 799-804.
  49. Kingery, W., *Densification during sintering in the presence of a liquid phase. I. Theory*. Journal of Applied Physics, 1959. **30**(3): p. 301-306.
  50. Shimoda, K., et al., *High-temperature mechanical property improvements of SiC ceramics by NITE process*. Materials transactions, 2006. **47**(4): p. 1204-1208.
  51. Bernachy-Barbe, F., et al., *Anisotropic damage behavior of SiC/SiC composite tubes: Multiaxial testing and damage characterization*. Composites Part A: Applied Science and Manufacturing, 2015. **76**: p. 281-288.

52. Zhang, J., et al., *Thermal diffusivity measurement of curved samples using the flash method*. Ceramic Materials for Energy Applications V: Ceramic Engineering and Science Proceedings, Volume 36, 2015(7): p. 43.
53. Singh, G., et al., *Interlaboratory Round Robin Study on Axial Tensile Properties of SiC/SiC Tubes*. 2017, Oak Ridge National Laboratory. p. ORNL/TM-2017/397.
54. Hayasaka, D., et al., *Gas leak tightness of SiC/SiC composites at elevated temperature*. Fusion Engineering and Design, 2016. **109**: p. 1498-1501.
55. Feinroth, H., et al. *Mechanical strength of CTP Triplex SiC fuel clad tubes after irradiation in MIT research reactor under PWR coolant conditions*. in *Ceramic Engineering and Science Proceedings*. 2009.
56. Park, J.-S., et al., *Efforts on large scale production of NITE-SiC/SiC composites*. Journal of Nuclear Materials, 2007. **367**: p. 719-724.
57. Fitriani, P., et al., *Fabrication of tubular SiC f/SiC using different preform architectures by electrophoretic deposition and hot pressing*. Ceramics International, 2017. **43**(10): p. 7618-7626.
58. Rohmer, E., E. Martin, and C. Lorrette, *Mechanical properties of SiC/SiC braided tubes for fuel cladding*. Journal of Nuclear Materials, 2014. **453**(1): p. 16-21.
59. Alva, L., et al., *Experimental study of thermo-mechanical behavior of SiC composite tubing under high temperature gradient using solid surrogate*. Journal of Nuclear Materials, 2015. **466**: p. 698-711.
60. Terrani, K.A., et al., *Progress on matrix SiC processing and properties for fully ceramic microencapsulated fuel form*. Journal of Nuclear Materials, 2015. **457**: p. 9-17.
61. Snead, L.L., et al., *Handbook of SiC properties for fuel performance modeling*. Journal of nuclear materials, 2007. **371**(1): p. 329-377.
62. Yamamoto, Y., et al., *Re-evaluation of SiC permeation coefficients at high temperatures*. Fusion Engineering and Design, 2016. **109**: p. 1286-1290.
63. Katoh, Y., et al., *Observation and possible mechanism of irradiation induced creep in ceramics*. Journal of Nuclear Materials, 2013. **434**(1): p. 141-151.
64. Hu, X., et al., *Determination of He and D permeability of neutronirradiated SiC tubes to examine the potential for release due to microcracking*. 2017, Oak Ridge National Laboratory.
65. Nozawa, T., et al., *Determination and prediction of axial/off-axial mechanical properties of SiC/SiC composites*. Fusion Engineering and Design, 2012. **87**(5): p. 803-807.
66. Terrani, K.A., et al., *Hydrothermal corrosion of SiC in LWR coolant environments in the absence of irradiation*. Journal of Nuclear Materials, 2015. **465**: p. 488-498.
67. Kim, D., et al., *Effect of dissolved hydrogen on the corrosion behavior of chemically vapor deposited SiC in a simulated pressurized water reactor environment*. Corrosion Science, 2015. **98**: p. 304-309.
68. Kim, H.-G., et al., *Adhesion property and high-temperature oxidation behavior of Cr-coated Zircaloy-4 cladding tube prepared by 3D laser coating*. Journal of Nuclear Materials, 2015. **465**: p. 531-539.
69. Brachet, J., et al., *On-going studies at CEA on chromium coated zirconium based nuclear fuel claddings for enhanced Accident Tolerant LWRs Fuel*.
70. Idarraga-Trujillo, I., et al. *Assessment at CEA of coated nuclear fuel cladding for LWRs with increased margins in LOCA and beyond LOCA conditions*. in *Conference Paper) LWR Fuel Performance Meeting, Top Fuel 2013*. 2013.
71. Alat, E., et al., *Ceramic coating for corrosion (c3) resistance of nuclear fuel cladding*. Surface and Coatings Technology, 2015. **281**: p. 133-143.
72. Wiklund, U., et al., *Multilayer coatings as corrosion protection of Zircaloy*. Surface and Coatings Technology, 1996. **86**: p. 530-534.
73. Daub, K., R. Van Nieuwenhove, and H. Nordin, *Investigation of the impact of coatings on corrosion and hydrogen uptake of Zircaloy-4*. Journal of Nuclear Materials, 2015. **467**: p. 260-270.

74. Zhong, W., et al., *Performance of iron–chromium–aluminum alloy surface coatings on Zircaloy 2 under high-temperature steam and normal BWR operating conditions*. Journal of Nuclear Materials, 2016. **470**: p. 327-338.
75. Van Nieuwenhove, R., et al., *In-pile testing of CrN, TiAlN and AlCrN coatings on Zircaloy cladding in the Halden Reactor*, in *18th International Symposium on Zirconium in the Nuclear Industry*. 2016: Hilton Head Island, SC, USA.
76. Braun, J., et al., *Chemical compatibility between UO<sub>2</sub> fuel and SiC cladding for LWRs. Application to ATF (Accident-Tolerant Fuels)*. Journal of Nuclear Materials, 2017. **487**: p. 380-395.
77. Silva, C.M., et al., *Chemical reactivity of CVC and CVD SiC with UO<sub>2</sub> at high temperatures*. Journal of Nuclear Materials, 2015. **460**: p. 52-59.
78. Gerczak, T.J., *Discussion of potential fuel cladding chemical interactions in LWR designs utilizing SiC/SiC cladding*, in *40th International Conference & Exposition on Advanced Ceramics & Composites*. 2015: Daytona Beach, Florida, USA.
79. Park, D.J., et al., *Oxidation behavior of silicon carbide at 1200 C in both air and water–vapor-rich environments*. Corrosion Science, 2014. **88**: p. 416-422.
80. Avincola, V.A., et al., *Oxidation at high temperatures in steam atmosphere and quench of silicon carbide composites for nuclear application*. Nuclear Engineering and Design, 2015. **295**: p. 468-478.
81. Lee, Y., et al., *Oxidation behavior of sintered tubular silicon carbide in pure steam I: Experiments*. Ceramics International, 2016. **42**(1): p. 1916-1925.
82. Cheng, T., et al., *Oxidation of fuel cladding candidate materials in steam environments at high temperature and pressure*. Journal of Nuclear Materials, 2012. **427**(1): p. 396-400.
83. Ben-Belgacem, M., et al., *Thermo-mechanical analysis of LWR SiC/SiC composite cladding*. Journal of Nuclear Materials, 2014. **447**(1): p. 125-142.
84. Petrie, C.M., et al., *Experimental design and analysis for irradiation of SiC/SiC composite tubes under a prototypic high heat flux*. Journal of Nuclear Materials, 2017.
85. Koyanagi, T. and Y. Katoh, *Mechanical properties of SiC composites neutron irradiated under light water reactor relevant temperature and dose conditions*. Journal of Nuclear Materials, 2017.
86. Snead, L., S. Zinkle, and D. White, *Thermal conductivity degradation of ceramic materials due to low temperature, low dose neutron irradiation*. Journal of Nuclear Materials, 2005. **340**(2): p. 187-202.
87. Snead, L.L., Y. Katoh, and S. Connery, *Swelling of SiC at intermediate and high irradiation temperatures*. Journal of Nuclear Materials, 2007. **367**: p. 677-684.
88. Katoh, Y., et al., *High-dose neutron irradiation of Hi-Nicalon Type S silicon carbide composites. Part 2: Mechanical and physical properties*. Journal of Nuclear Materials, 2015. **462**: p. 450-457.
89. Koyanagi, T., et al., *Effects of neutron irradiation on mechanical properties of silicon carbide composites fabricated by nano-infiltration and transient eutectic-phase process*. Journal of Nuclear Materials, 2014. **448**(1): p. 478-486.
90. Katoh, Y., et al., *Thermophysical and mechanical properties of near-stoichiometric fiber CVI SiC/SiC composites after neutron irradiation at elevated temperatures*. Journal of Nuclear Materials, 2010. **403**(1): p. 48-61.
91. Newsome, G., et al., *Evaluation of neutron irradiated silicon carbide and silicon carbide composites*. Journal of Nuclear Materials, 2007. **371**(1): p. 76-89.
92. Koyanagi, T., et al., *Irradiation resistance of silicon carbide joint at light water reactor–relevant temperature*. Journal of Nuclear Materials, 2017. **488**: p. 150-159.
93. Henager, C.H., et al., *Modeling and testing miniature torsion specimens for SiC joining development studies for fusion*. Journal of Nuclear Materials, 2015. **466**: p. 253-268.
94. Goglio, L. and M. Ferraris, *Bonding of ceramics: An analysis of the torsion hourglass specimen*. International Journal of Adhesion and Adhesives, 2016. **70**: p. 46-52.

95. Burns, W. and P. Moore, *Water radiolysis and its effect upon in-reactor zircaloy corrosion*. Radiation Effects, 1976. **30**(4): p. 233-242.
96. Kondo, S., et al., *Effect of irradiation damage on hydrothermal corrosion of SiC*. Journal of Nuclear Materials, 2015. **464**: p. 36-42.